



Norwegian University of
Science and Technology

Heat generation and conduction in combined ultrasound imaging and therapy transducers

Britt Ingunn Nydal

Master of Science in Mechanical Engineering

Submission date: July 2017

Supervisor: Ivar Ståle Ertesvåg, EPT

Co-supervisor: Bjørn Atle Angelsen, Institutt for sirkulasjon og bildediagnostikk
Ola Finneng Myhre, Institutt for sirkulasjon og bildediagnostikk

Norwegian University of Science and Technology
Department of Energy and Process Engineering

EPT-M-2017-57

MASTER THESIS

for

Student Britt Ingunn Nydal
Spring 2017**Heat generation and conduction in combined ultrasound imaging and therapy transducers***Varmeutvikling og varmeleiing i transduserar for kombinert biletgjering og terapi*

Background: Ultrasound waves are interesting for mediation of drug delivery to tumors, where

- i) a high frequency (e.g. ~ 10 MHz) ultrasound provides an acoustic radiation force that can be used to increase transport of drugs from the capillaries and deep into the tissue interstitium to reach the cancer cells, and
- ii) low frequency (e.g. ~ 1 MHz) can be used to produce stable cavitation of intra-venously injected micro bubbles to open biological membranes (e.g. a cell membrane) for improved transport of drugs and genes across membranes
- iii) low frequency (e.g. ~ 1 MHz) can be used to break nano particle drug carriers to release the drug molecules within the tumor and protect normal tissue.

For these applications there is a need for high power, multifrequency ultrasound transducers. High power transmit requires that the thermal losses in the transducer is minimized, which in current transducer designs is obtained with a low electro-acoustic conversion bandwidth. It is also interesting to use such multi-frequency transducers for imaging of cancer tumors with the SURF technique, which requires large electro-acoustic conversion bandwidth. With current large bandwidth transducer designs there is considerable thermal power losses in the transducer, which makes high power transmit for drug delivery difficult.

Goal: The project goal is initial work on studying heat sources and heat transport in vibrating multi band transducers with adequate bandwidths to be used both for ultrasound imaging and for mediation of drug delivery. Numerical simulations shall be used to give insight into how cooling systems might allow for combined wide band imaging and high power drug delivery transducers.

The following tasks are to be considered:

- * Figure out a suitable simulation method and domain for simulation of heat transfer in a multifrequency ultrasound transducer.
- * Study the relation between heat generation in transducers and generated acoustic intensity in therapeutic applications, taking into account transducer geometry and focusing.
- * In cooperation with supervisors, define a series of cases to investigate. Conduct these investigations.
- * Discuss the limiting factors of heat transfer in multifrequency transducers and identify parameters that are critical in limiting internal temperature.
- * Discuss potential practical methods for the transport of heat from the heat-draining layer in a transducer.

-- ” --

Within 14 days of receiving the written text on the master thesis, the candidate shall submit a research plan for his project to the department.

When the thesis is evaluated, emphasis is put on processing of the results, and that they are presented in tabular and/or graphic form in a clear manner, and that they are analyzed carefully.

The thesis should be formulated as a research report with summary both in English and Norwegian, conclusion, literature references, table of contents etc. During the preparation of the text, the candidate should make an effort to produce a well-structured and easily readable report. In order to ease the evaluation of the thesis, it is important that the cross-references are correct. In the making of the report, strong emphasis should be placed on both a thorough discussion of the results and an orderly presentation.

The candidate is requested to initiate and keep close contact with his/her academic supervisor(s) throughout the working period. The candidate must follow the rules and regulations of NTNU as well as passive directions given by the Department of Energy and Process Engineering.

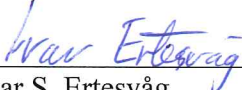
Risk assessment of the candidate's work shall be carried out according to the department's procedures. The risk assessment must be documented and included as part of the final report. Events related to the candidate's work adversely affecting the health, safety or security, must be documented and included as part of the final report. If the documentation on risk assessment represents a large number of pages, the full version is to be submitted electronically to the supervisor and an excerpt is included in the report.

Pursuant to "Regulations concerning the supplementary provisions to the technology study program/Master of Science" at NTNU §20, the Department reserves the permission to utilize all the results and data for teaching and research purposes as well as in future publications.

The final report is to be submitted digitally in DAIM. An executive summary of the thesis including title, student's name, supervisor's name, year, department name, and NTNU's logo and name, shall be submitted to the department as a separate pdf file. Based on an agreement with the supervisor, the final report and other material and documents may be given to the supervisor in digital format.

- Work to be done in lab (Water power lab, Fluids engineering lab, Thermal engineering lab)
 Field work

Department of Energy and Process Engineering, 9 February 2017



Ivar S. Ertesvåg
Academic Supervisor

Co-Supervisor(s):

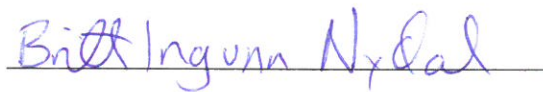
Bjørn Atle J. Angelsen, Professor, Department of Circulation and Medical Imaging
Ola Myhre, PhD candidate, Department of Circulation and Medical Imaging

Preface

This thesis is a result of my master degree at the Department of Energy and Process Engineering, NTNU. It accounts for 30 credits and is the last semester of the study program Mechanical Engineering.

I want to thank my supervisor Professor Ivar Ståle Ertesvåg and my co-supervisors Professor Bjørn Angelsen and ph.D. Candidates Ola Myhre and Ole Brende, at the Department of Circulation and Medical Imaging, for their help and support.

Trondheim 09.07.2017



Britt Ingunn Nydal

Summary

In this thesis, the heat sources and heat transfer in high power, multifrequency transducers to be used for both ultrasound imaging and mediation of drug delivery, are studied.

Electrical energy is converted into acoustic energy in a transducer, and in this process, due to acoustic energy absorption, some energy is also converted to thermal energy. With higher frequency, these heat sources are larger, and it can lead to overheating of the transducer. A 9 MHz probe is used in this project, and the heat sources are calculated in the program x-trans.

In the transducer, we have conduction in the layers and convective heat transfer between the transducer and the surroundings. Radiation is neglected in the simulations. The heat transfer is simulated using the software Comsol Multiphysics.

The results show that the temperature development in the transducer in the first 10 seconds of usage is transient or unsteady. The internal energy generation is larger than the convection rates with the surroundings. The highest temperature in the transducer is measured in the matching layers, which are on the face, with a value of 336.8 K for the transducer used today. The real temperature rise, with a temperature of 381 K, happens in the load, which is the body of the patient. The critical parameter in limiting internal temperature is the heat source in the load.

Some different transducer geometries are tested in order to see how it affects the temperature distribution. The geometry with the largest backing layer is measured to have the lowest maximum temperature in the transducer. The temperature is measured as 310.3 K in the transducer and 379.4 K in the load. Also, the use of fans to cool the transducer is simulated, in addition to a heat sink method that consists of copper slabs. Based on the simulations, the slabs are most effective in cooling the transducer. The temperature is measured as 314 K in the transducer, and 366.8 K in the load.

Sammendrag

I denne oppgaven er varmekilder og varmeutvikling i multifrekvens transducere med høy effekt simulert. De skal både blir brukt til ultralydabildning og terapi.

I en transducer blir elektrisk energi overført til akustisk energi, men i denne prosessen blir også noe energi overført til termisk energi. I denne studien blir en 9 MHz probe brukt. Med en så høy frekvens blir varmekildene store og det kan føre til for høy temperatur i transduceren. Varmekildene er beregnet i programmet x-trans.

I transduceren skjer det varmeutvikling ved konduksjon i lagene, og i tillegg er det konveksjon mellom transduceren og omgivelsene. Stråling er neglisjert i disse simuleringene. Ved hjelp av programmet Comsol Multiphysics er varmeutviklingen simulert.

Resultatene viser at varmeutviklingen de første 10 sekundene i transduceren er transient. Det betyr at varmegenereringen i transduceren er større enn varmeutviklingen mellom transduceren og omgivelsene. Den høyeste temperaturen i transduceren er på enden av transduceren, i ”matching”-lagene, og for en modell av en transducer brukt i dag er den beregnet til å være 336.8 K. Den virkelige temperaturøkningen skjer i lasten som er kroppen til pasienten med en temperatur på 381 K. Den kritiske parameteren til å begrense temperaturen er varmekilden i lasten.

Forskjellige geometrier av transduceren er simulert for å se hvordan det påvirker varmeutviklingen. Resultatene viser at geometrien med det største ”backing”-laget har den laveste maximumtemperaturen i transduceren. Temperaturen er beregnet til å være 310.3 K i transduceren og 379.4 K i lasten. I tillegg er transducer med vifte og kobberskiver simulert for å se hvordan effekt det har på avkjøling av transduceren. Basert på simuleringene er kobberskivene mest effektive av de to metodene og gir dermed de laveste temperaturene. I transduceren er temperaturen beregnet til å være 314 K og i lasten 366.8 K.

Contents

1	Introduction	7
1.1	Background	7
1.2	Motivation	7
1.3	Organization of the report	8
2	Theory	9
2.1	Ultrasound	9
2.1.1	Ultrasound imaging	9
2.1.2	Ultrasound as therapy	9
2.1.3	The ultrasonic transducer	10
2.1.4	SURF imaging	11
2.2	Ultrasound radiation force	12
2.2.1	Energy in acoustic waves	17
2.3	Heat transfer	19
2.3.1	Conduction	19
2.3.2	Steady-state conduction	21
2.3.3	The heat diffusion equation	22
2.3.4	Transient conduction	24
2.3.5	Convection	28
2.3.6	Radiation	30
2.3.7	Thermal resistance	32
2.3.8	Thermal contact resistance	33
2.3.9	Boundary and initial conditions	34
2.3.10	Cooling methods	35
3	Simulation tool	37
3.1	The finite element method	37
3.1.1	Ordinary and partial differential equations	38
3.1.2	Basic functions and test functions	39
3.1.3	Finite element mesh refinement	40
3.1.4	Mathematical model and numerical model	41
3.1.5	Errors in finite element analysis	41
3.2	Transport phenomena	42
3.2.1	Conservation of energy	42

3.2.2	Tolerances for a time dependent problem	43
4	Thermal design: development and analysis	45
4.1	Geometry	46
4.2	Materials	47
4.2.1	Copper	47
4.2.2	Epoxy	47
4.2.3	Piezoelectric ceramic	48
4.3	Domain settings, boundary conditions and initial conditions . . .	50
4.4	Mesh	51
4.5	Simulation setup	52
4.5.1	Heat generation	52
4.5.2	Heat development	52
4.5.3	Cooling methods	57
5	Results	59
5.1	Heat generation	59
5.2	Heat development	61
5.3	The different geometries	63
5.4	Transducer with fans	69
5.4.1	Transducer with copper slabs	71
6	Discussion	75
6.1	Steady-state	75
6.2	Estimation of heat loss	75
6.3	The limiting factors of heat transfer	76
6.4	Influence of the materials	76
6.5	Influence of the fans	77
6.6	Influence of the copper slabs	77
6.7	Radiation	77
7	Conclusion	79

1. Introduction

1.1 Background

In recent years, mediation of drug delivery to tumors using ultrasound waves has been appearing as an interesting therapeutic choice for cancer treatment. With the properties of small particle size and long circulation time, nanocarriers have been used for the drug delivery. Nanocarriers can pass through cell membrane walls and blood capillary walls to deliver drugs [Zhou et al., 2014]. The mechanisms of the interaction between nanocarriers and ultrasound is related to cavitation, thermal effects and mechanical effects. With these mechanisms, cell death and disruption of tissue structure may occur [Zhou et al., 2014]. This new technology has the potential for becoming a powerful technique in many aspects related to imaging and therapy of cancer. However, there are several challenges that must be overcome first.

To get the best performance of the ultrasound transducer it has to be capable of operating at high acoustic intensities [Hart, 2006]. With this, in addition to the continuous usage of the transducer, one of the problems is when it gets a higher temperature than the operating range. For the transducer, this temperature range is given by three constraints. The first is a temperature limit for patient contact. The second requirement is related to the operators comfort and safety. The third is due to a maximum temperature limit for the electronics in the transducer. Also, when the technology is evolving the need for more thermal management techniques are needed to cool the ultrasound transducer [Park et al., 2008].

1.2 Motivation

This thesis is part of a project at the Norwegian University of Science and Technology (NTNU) where ultrasound waves are used to create mediation of drug delivery to tumors. The focus in this report will be on studying heat generation in multifrequency ultrasound transducers operating at high acoustic intensities to be used for both ultrasound imaging and mediation of drug delivery. The

multifrequency technique used is called SURF Imaging where both high and low frequency waves are transmitted at the same time. This report is primarily written for people with other areas of expertise than heat transfer.

1.3 Organization of the report

First, the heat loss due to acoustic energy absorption in the transducer will be studied. Then, numerical simulations will be used to give insight in the heat generation and the factors that are critical in limiting internal temperature. Potential practical methods for the transport of heat will be simulated and discussed in the end.

2. Theory

In this section I will outline some theory to understand the following chapters. Initially, general ultrasound theory will be presented along with description of plane waves. Then, the basic heat transfer phenomena and cooling methods are summarized.

2.1 Ultrasound

2.1.1 Ultrasound imaging

Medical ultrasound imaging uses sound waves with a high frequency (e.g. 10 MHz) for visualizing and diagnosing the condition and health inside a human body. It is used in many clinical applications today. The images are captured in real-time, and it can therefore show the movement of internal organs and blood flowing through vessels [Cole et al., 2011].

To produce an image, ultrasound waves are transmitted from a transducer into the body in different directions. The waves are reflected off the body structures because of the varying density of the medium, and the echoes give the information that is used to produce images. The information necessary in an ultrasound exam is the time it takes for the wave to travel through the body. Ultrasound imaging does not expose you to radiation, unlike x-ray, and it is a quick, painless and safe method, even for such uses as fetal imaging [Szabo, 2004].

2.1.2 Ultrasound as therapy

Traditionally, for many solid tumours, surgery has been the only cure. Open surgery has been replaced by less invasive techniques over the years and the technological advances are still evolving. Minimally invasive surgery has become more and more common, but because high-intensity focused ultrasound (HIFU) is a noninvasive emerging technique it has the potential for becoming a more powerful tool in many aspects related to both cancer imaging and therapy [Kaneko and Willmann, 2012]. HIFU does not have as many side effects as other types of cancer treatments already in use because only sound waves are used to

destroy the cancer cells. In the 1930s the medical uses of ultrasound for therapy were initially explored, and HIFU was first studied in the 1950s [Kennedy, 2005].

An ultrasound probe can be used to deposit energy in tissue to promote various biological effects. When the probe is manufactured into an arc shape, intersecting beams of ultrasound can be focused at a focal spot and produce high local intensities [Miller et al., 2012]. For therapy, ultrasonic energy can induce effects through heating, ultrasonic cavitation, mechanical stress among others.

There are some risks with therapeutic ultrasound. When delivering ultrasonic energy, it is always a consideration with undesired tissue injury. Unwanted burns and pain can occur. Safety is an important consideration when introducing HIFU applications to clinical practice [Miller et al., 2012].

Because HIFU involves delivering ultrasonic energy at localized areas it can only treat a single tumour or part of a large tumour. Also because HIFU can not travel through air or solid bone, it can not treat every type of cancer or cancer that has spread to more places in the body [HIF, 2015].

2.1.3 The ultrasonic transducer

The device converting electrical energy into acoustic energy is the piezoelectric transducer. Piezoelectric materials consist of crystals of polar molecules which lack centers of symmetry. Direct piezoelectric effect is the phenomenon when a voltage develops between the two faces of a plate if a plate cut from such a crystal is mechanically deformed [Angelsen, 2000]. Driving the plate with an oscillating voltage makes the plate to vibrate. The vibrations excite an acoustic pressure wave into the biological material in contact with the front face of the plate. When an acoustic wave hits the plate, the plate functions as a receiver. It excites vibrations in the plate which generates a voltage between the electrodes.

A piezoelectric ultrasound transducer can be made as an elastic plate of piezoelectric material with one or more acoustic matching layers mounted on a backing material. It is also connected to the load material as shown in Figure 2.1. Thin electrodes for applying an electrical voltage are metallized on the surfaces of the plate.

The function of the backing material is attenuating acoustic energy which is directed backwards to minimize reverberations, and as a mechanical support for the piezoelements [Park et al., 2008]. On top of the transducer there are matching layers to transform between the high and the low acoustic impedance in the piezoelements. The matching layers are also limiting reflection of acoustic waves from the load.

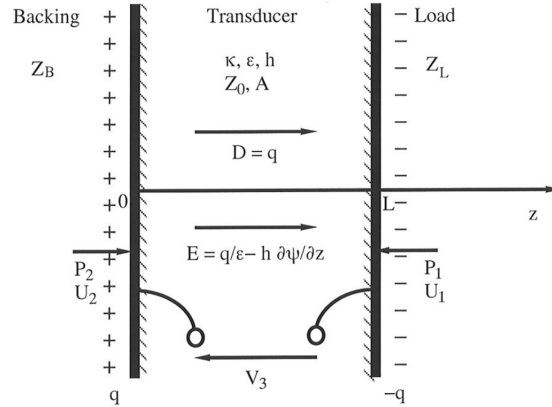


Figure 2.1: Cross section of a piezoelectric plate [Angelsen, 2000]

Materials with strong piezoelectric properties are found in ceramic composites of lead, zirconates and titanates [Zhang et al., 2017]. Lead zirconate titanate is often used, but this material has generally poor thermal conductivity.

When the transducer performs its functions, there are practical and regulatory limits on the allowable surface temperature. Increased internal temperatures may also reduce the efficiency of the transducer and/or the operating capabilities. When measured in air the Underwriters Laboratory "Standard for Safety: Medical and Dental Equipment" for example species an upper limit of 323 K. When tested against a tissue mimicking material the upper limit was set to 316 K for the transducer portion contacting the patient's skin [Hart, 2006].

2.1.4 SURF imaging

Second order ultrasound field (SURF) Imaging is a technique based on transmitting a low frequency (LF) wave and a high frequency (HF) wave at the same time in the same direction [Angelsen, 2000]. The LF wave is typically at 0.2 MHz to 1.2 MHz and the HF wave at 1.0 MHz to 10.0 MHz. With high radiation force, the HF pulse can be used to increase the transport of drugs that reaches the cancer cells [Eggen et al., 2014]. The LF pulse can be used to improve transport of drugs across membranes by producing stable cavitation of injected nanocarriers. In addition, the LF pulse can be used to break the nanocarriers to release the drug molecules within the tumor and protect normal tissue. With the SURF Imaging technique, the spatial resolution in conventional ultrasound imaging is improved, and it offers a range of new possibilities.

2.2 Ultrasound radiation force

Plane waves are waves with phase fronts that are planes in three-dimensional space and where the energy propagates in a linear direction [Angelsen, 2000]. Plane waves do not exist in practical life, but it can serve as an approximation for a limited region of space when the transversal dimensions can be assumed to be infinite as an example.

An ultrasound transducer generates plane, longitudinal pressure waves into the bulk of the biological material. Longitudinal waves means that the particle motion is along the propagation direction of the wave. The biological material can be viewed as an isotropic and homogeneous elastic material. Isotropic means that the properties are independent of the direction, while homogeneous means that the material properties are constant in space [Angelsen, 2000].

The ultrasound waves can be reflected, absorbed, refracted and focused. They are not absorbed much by water and other tissues and therefore, the waves can transmit energy into cells. The waves causes cyclic compressions and expansions. In Figure 2.2, we see two fictitious planes, I_1 and I_2 , in the elastic material which are normal to the direction of the wave propagation. The wave motion will cause the planes to vibrate. The displacement of the plane, $\psi(z, t)$, from its equilibrium position x are shown in the figure. At any time, the vibration velocity and acceleration of the plane can be consequently written as

$$u(z, t) = \frac{\partial \psi(z, t)}{\partial t}, \quad (2.1)$$

$$a(z, t) = \frac{\partial u(z, t)}{\partial t} = \frac{\partial^2 \psi(z, t)}{\partial t^2}. \quad (2.2)$$

This is the Lagrangian description which, in contrast to the Euler description, is based on relating the displacement of a particle in space to an equilibrium position. The equilibrium position is the position where no forces are acting upon the particle.

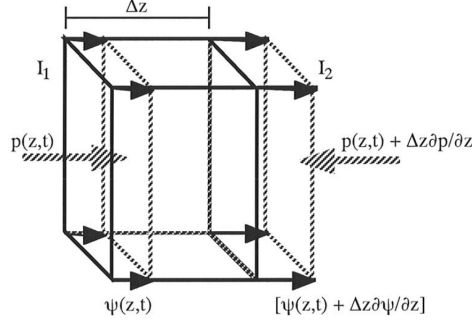


Figure 2.2: Volume change of a thin element of a material caused by the wave motion [Angelsen, 2000]

Pressure, $p(z, t)$, is generated on the plane when the variations of ψ along the propagation direction causes a compression or an expansion of the medium. The linearized volume compression of the element is defined as

$$\delta V = [\psi(z, t) + \Delta z \frac{\partial \psi(z, t)}{\partial z} - \psi(z, t)]A. \quad (2.3)$$

Then we can get the relative volume compression as

$$\frac{\delta V}{\Delta V} = \frac{\partial \psi}{\partial z}, \quad (2.4)$$

where the unstrained volume is $\Delta V = \Delta z A$. The acoustic pressure on the plane can be written as

$$p \approx -\frac{1}{\kappa} \frac{\partial \psi}{\partial z}, \quad (2.5)$$

where κ is the compressibility of the fluid. Differentiating with respect to time, Eq. 2.27 can be written as

$$\frac{\partial p(z, t)}{\partial t} = -\frac{1}{\kappa} \frac{\partial u}{\partial z}. \quad (2.6)$$

The negative pressure gradient gives the net force of the volume element between the two planes I_1 and I_2 , written as

$$\Delta F = [p(z, t) - (p(z, t) + \Delta z \frac{\partial p(z, t)}{\partial z})]A, \quad (2.7)$$

$$\Delta F = -\frac{\partial p(z, t)}{\partial z} \Delta z A = -\frac{\partial p(z, t)}{\partial z} \Delta V, \quad (2.8)$$

where I_1 is at z and I_2 is at $z + \Delta z$. The volume of the unstrained element is $\Delta V = \Delta z A$.

D'Alembert gives the solution of the one-dimensional wave equation as

$$u(z, t) = U_+(z - ct) + U_-(z + ct), \quad (2.9)$$

$$p(z, t) = P_+(z - ct) + P_-(z + ct), \quad (2.10)$$

where the arbitrary functions U_+ , U_- , P_+ and P_- represents waves propagating in the positive and the negative z -direction shown in Figure 2.3.

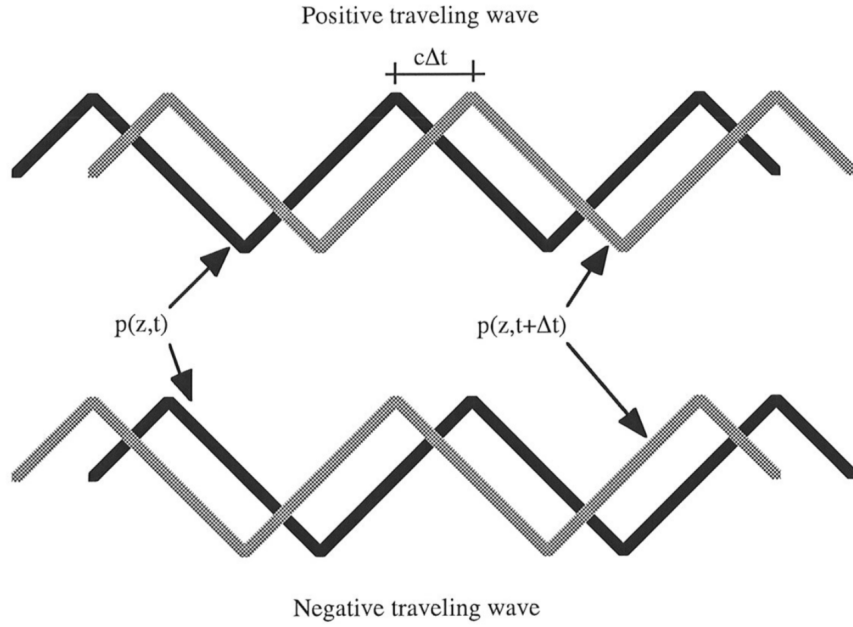


Figure 2.3: Positive and negative propagating waves [Angelsen, 2000]

Between two semi-infinite materials with characteristic impedance I_1 and I_2 , we are assuming an interface at $z = 0$. As shown in Figure 2.4 a wave in the left material propagates from left to the right. When it hits the interface, the wave will be partially reflected and partially transmitted. The reflection coefficient, R_{01} , can be calculated as

$$R_{01} = \frac{P_{0-}}{P_{0+}} = \frac{Z_1 - Z_0}{Z_0 + Z_1} = -\frac{U_{0-}}{U_{0+}}, \quad (2.11)$$

and the transmission coefficient, T_{01} , as

$$T_{01} = \frac{P_{1+}}{P_{0+}} = \frac{2Z_1}{z_0 + Z_1}. \quad (2.12)$$

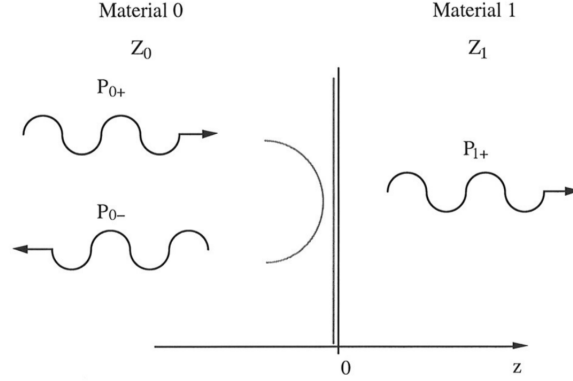


Figure 2.4: Reflections of a plane wave at the boundary between two materials [Angelsen, 2000]

In the left material the pressure and the particle velocity at $z = 0$ will be

$$P_0 = P_{0+} + P_{0-}, \quad (2.13)$$

$$U_0 = \frac{P_{0+}}{Z_0} - \frac{P_{0-}}{Z_0}. \quad (2.14)$$

The pressure and the particle velocity in the right material will be at the interface, respectively

$$P_1 = P_{1+}, \quad (2.15)$$

$$U_1 = \frac{P_{1+}}{Z_1}. \quad (2.16)$$

The wave function can also be written as

$$p(z, t) = Z_0[U_+(z - ct) - U_-(z + ct)], \quad (2.17)$$

where the characteristic mechanical/acoustic impedance, $Z_0 \text{ kg}/(\text{m}^2\text{s})$ of the material is defined as

$$Z = \frac{1}{\kappa c} = \rho c. \quad (2.18)$$

Then we can calculate the reflection coefficient, R_{01} , as

$$R_{01} = \frac{P_{0-}}{P_{0+}} = \frac{Z_1 - Z_0}{Z_0 + Z_1} = \frac{U_{0-}}{U_{0+}}, \quad (2.19)$$

and the transmission coefficient, T_{01} , as

$$T_{01} = \frac{P_{1+}}{P_{0+}} = \frac{2Z_1}{Z_0 + Z_1}. \quad (2.20)$$

When $Z \Rightarrow \infty$ and $Z \Rightarrow 0$ we get total reflection with $R_{01} = 1$ and $R_{01} = -1$ respectively. When the wave propagates from a material with high impedance

to a material with low impedance, the particle velocity is increased and the pressure is reduced. The opposite is happening when the wave is travelling from a material with low impedance to a material with high impedance.

In Figure 2.5 we have a plate submersed in two semi-infinite materials with a wave coming from the left infinity in Material 1. The wave is partially reflected and partially transmitted at the interface between material 1 and material 0. Again, the wave is partially reflected and transmitted at the interface to material 2.

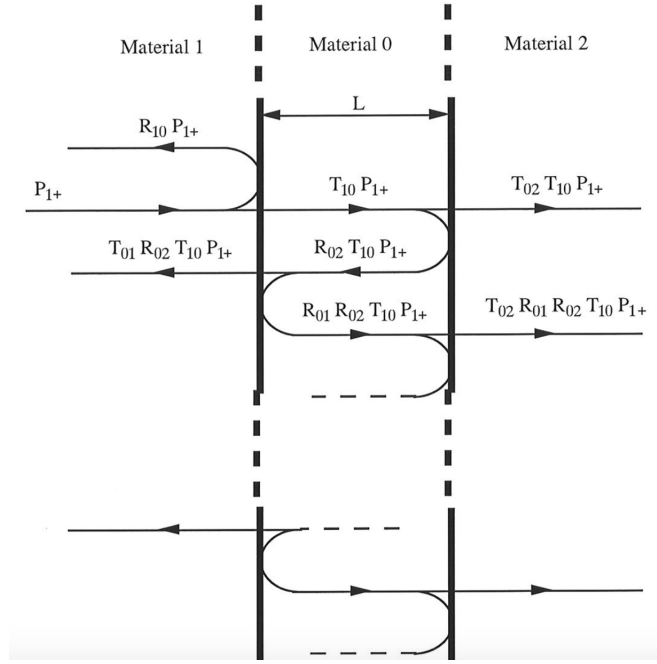


Figure 2.5: Multiple reflections of an incoming wavefront [Angelsen, 2000]

The reflection and transmission coefficients between material 1 and material 0 can be written as

$$R_{10} = \frac{Z_0 - Z_1}{Z_1 + Z_0}, \quad (2.21)$$

$$T_{10} = \frac{2Z_0}{Z_1 + Z_0}. \quad (2.22)$$

Likewise, the reflection and the transmission coefficients from material 0 to material 2 are defined as

$$R_{02} = \frac{Z_2 - Z_0}{Z_0 + Z_2}, \quad (2.23)$$

$$T_{02} = \frac{2Z_2}{Z_0 + Z_2}. \quad (2.24)$$

We will have partial reflections back and forth in material 0 as the figure shows. Every time the wave hits the left interface it will generate a transmitted partial wave that propagates leftwards in material 1, and every time the wave hits the right interface it will generate a transmitted partial wave that propagates rightwards in material 2.

2.2.1 Energy in acoustic waves

There are two fundamental energy forms in the acoustic wave motion, kinetic energy of the particle velocity and potential energy given by the volume compression. With loss of energy from the acoustic wave, energy will be converted to other energy forms like heat and chemical energy. This energy conversion is termed acoustic energy absorption.

To analyze the energy transfer in the wave motion we are considering the volume element in Figure 2.2. There is a change of energy during a short time interval dt given by the product of the displacement of the faces and the force on the faces. The work done on the volume element by the external medium is

$$dW_1 = pAuds. \quad (2.25)$$

Through the right side, the work done is

$$dW_2 = -[p + \frac{\partial p}{\partial z}\Delta z]A[u + \frac{\partial u}{\partial z}\Delta z]ds. \quad (2.26)$$

If the external energy from the work of pressure on the faces is added to the volume element, we get

$$dW = dW_1 + dW_2 = -\Delta zA\frac{\partial p}{\partial z}uds - \Delta zAp\frac{\partial u}{\partial z}ds = -\Delta A\frac{\partial(pu)}{\partial z}ds. \quad (2.27)$$

This energy is used to build up acoustic wave energy, dE , in the volume element, but some of the energy is also converted to heat, dQ . The energy equation can be expressed as

$$dW = dE + dQ. \quad (2.28)$$

The conservation of energy can be the exchange of energy through either heat conduction or viscous friction. The conversion can also go through relaxation type processes to irragainable forms of energy within the volume element. The conversation to nonregainable heat can be expressed as

$$dQ = q\Delta Vds, \quad (2.29)$$

where $q(z, t)$ is the heat current. Inserting Equation 2.27 and 2.28 into 2.29 we get the continuity equation for acoustic energy

$$-q' = \frac{\partial e}{\partial t} + \frac{\partial(pu)}{\partial z}. \quad (2.30)$$

The acoustic energy density, $e = E/\Delta$, is the acoustic energy pr. unit volume. The power transfer per unit area across an interface normal to the wave direction, $p \cdot u$, is often denoted as the radiation intensity, I , which is a vector with direction of the particle velocity

$$I(z, t) = p(z, t)u(z, t)e. \quad (2.31)$$

The acoustic energy density can be written as

$$e(z, t) = \frac{1}{2}\rho u^2(z, t) + \frac{1}{2}\kappa p^2(z, t), \quad (2.32)$$

where the first term in the equation represents the kinetic energy density and the second term represents the potential energy density [Angelsen, 2000]. Differentiating twice with respect to z , we get

$$\frac{\partial^2 e}{\partial z^2} = -\rho\kappa \frac{\partial^2(pu)}{\partial z \partial t} = \rho\kappa \frac{\partial^2 e}{\partial t^2} + \rho\kappa \frac{\partial^2 q}{\partial t^2}. \quad (2.33)$$

As this equation describes, energy density propagates according to Equation 2.35, which is the wave equation

$$c = \frac{1}{\sqrt{\rho\kappa}}, \quad (2.34)$$

$$\frac{\partial^2 e}{\partial z^2} - \frac{1}{c^2} \frac{\partial^2 e}{\partial t^2} = \frac{1}{c^2} \frac{\partial^2 q}{\partial t^2}. \quad (2.35)$$

2.3 Heat transfer

Heat transfer can be defined as the exchange of thermal energy due to a temperature difference between physical systems. The three fundamental types of heat transfer are conduction, convection and radiation, and they are shown in Figure 2.6. Conduction refers to the heat transfer due to random molecular motion. Convection occurs when we have a combination of diffusion and bulk movement of substances. The third concept is radiation and it refers to the emission of energy in the form of electromagnetic waves [Dewitt et al., 2007].

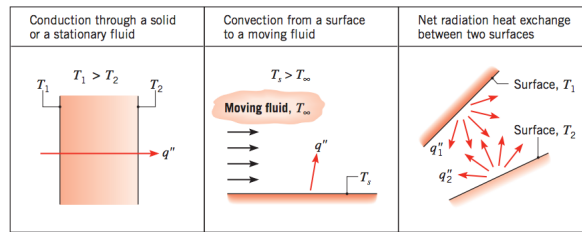


Figure 2.6: Conduction, convection, and radiation heat transfer modes [Dewitt et al., 2007]

2.3.1 Conduction

Conduction refers to the transport of energy due to interactions between the particles from the more energetic to the less energetic particles. Higher temperatures are associated with higher molecular energies, and thus the energy will transfer from the area of higher temperatures to the area with lower temperatures. The net transfer of energy by random molecular motion refers to a diffusion of energy. In a gas the energy transfer is attributed by collisions of molecules. We have the same situation in a liquid. However, the molecules are more closely spaced. In a solid the energy transfer is enhanced by atomic activity in the form of lattice vibrations.

The rate equation for heat conduction in the one-dimensional plane wall, having a temperature distribution $T(x)$, is expressed as

$$Q_x = -kA \frac{\partial T}{\partial x}. \quad (2.36)$$

This equation is called Fourier's law and is a cornerstone in conduction heat transfer. The constant, k , is a transport property called the thermal conductivity (W/mK) and is a characteristic of the wall material. A is the cross-sectional area. Rate equations may be used to compute the amount of energy transferred per unit time. The minus sign indicates that heat is transferred in the direction

of increasing temperature. Fourier's law is applicable to transient, multidimensional conduction in complex geometries.

The heat flux, q_x (W/m²), is the heat transfer rate in the x -direction per unit area perpendicular to the direction of transfer

$$q_x = \frac{Q_x}{A} = -k \frac{\partial T}{\partial x}. \quad (2.37)$$

The heat flux is a vector quantity, and in a more general form, Fourier's law can be written as

$$\mathbf{q} = -k\nabla T = -k\left(\mathbf{i} \frac{\partial T}{\partial x} + \mathbf{j} \frac{\partial T}{\partial y} + \mathbf{k} \frac{\partial T}{\partial z}\right) = q_x \mathbf{i} + q_y \mathbf{j} + q_z \mathbf{k}. \quad (2.38)$$

$T(x, y, z)$ is the temperature field and ∇ is a three-dimensional operator.

The thermal conductivity provides an indication of the rate at which energy is transferred by the diffusion process. The thermal conductivity depends on the physical structure of matter, atomic and molecular. In general, a solid has larger thermal conductivity than that of a liquid, which is larger than that of a gas. The thermal conductivity can vary by a factor of 10^5 between diamond and gases at room temperature, as shown in Figure 2.7. This is due largely to differences in intermolecular spacing for the two states.

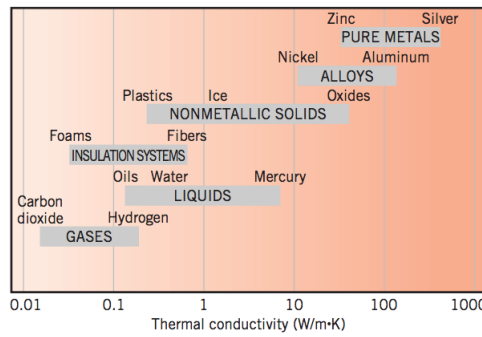


Figure 2.7: Range of thermal conductivity for various states of matter [Dewitt et al., 2007]

A material in the solid state may be comprised of atoms and free electrons in a lattice, periodic arrangement of the atoms bound in a material. The transportation of thermal energy can then be related to two effects, the lattice vibrational waves and the migration of free electrons. In pure metals, the electron contribution to conduction heat transfer is dominant, whereas in nonconductors and semiconductors, the phonon contribution dominates.

The thermal conductivity can be expressed as follows yielding the kinetic theory

$$k = \frac{1}{3} C \bar{c} \lambda_{mfp}, \quad (2.39)$$

where C is the electron specific heat per unit volume and \bar{c} is the mean electron velocity. λ_{mfp} is the mean free path of the electron and is defined as the average distance an electron travels before it collides with either a phonon or an imperfection in the material [Dewitt et al., 2007]. When the mean free path of the energy carriers increases, the thermal conductivity is increased.

The thermal conductivity can also vary with temperature. Figure 2.8 shows the temperature dependence of k for representative metallic and nonmetallic solids.

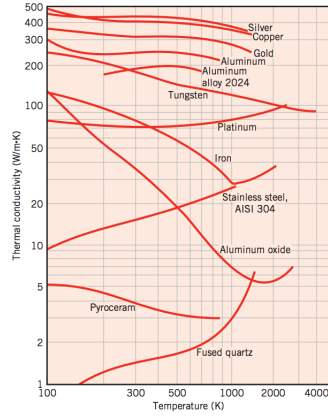


Figure 2.8: The temperature dependence of the thermal conductivity of selected solids [Dewitt et al., 2007]

2.3.2 Steady-state conduction

Under one-dimensional steady state conditions as shown in Figure 2.9, the temperature distribution varies linearly with x , if we consider constant conductivity, and the change in temperature may be expressed as

$$\frac{\partial T}{\partial x} = \frac{T_2 - T_1}{L}, \quad (2.40)$$

and the heat flux is then

$$q_x = k \frac{T_2 - T_1}{L} = k \frac{\Delta T}{L}. \quad (2.41)$$

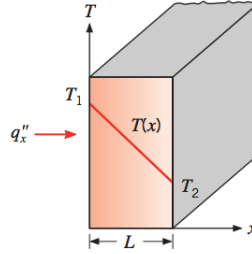


Figure 2.9: One-dimensional heat transfer by conduction [Dewitt et al., 2007]

The total heat rate by conduction through a plane wall of area A is then the product of the flux and the area, $Q_x = q_x \cdot A$.

2.3.3 The heat diffusion equation

The heat diffusion equation is the primary equation upon determining the temperature distribution in a medium, meaning how the temperature varies with position and time. It is obtained by combining the First Law of Thermodynamics and Fourier's law. The heat diffusion equation is a differential equation where the heat flux, q , is eliminated.

To obtain the heat diffusion equation we define a differential control volume $dx \cdot dy \cdot dz$ as shown in Figure 2.10. The temperature distribution $T(x, y, z)$ is expressed in Cartesian coordinates and there is no bulk motion in the homogeneous medium. We are only considering the thermal forms of energy. By the first law the conduction heat rates, shown in Figure 2.10, can be expressed as

$$q_{x+dx} = q_x + \frac{\partial q_x}{\partial x} dx, \quad (2.42)$$

$$q_{y+dy} = q_y + \frac{\partial q_y}{\partial y} dy, \quad (2.43)$$

$$q_{z+dz} = q_z + \frac{\partial q_z}{\partial z} dz. \quad (2.44)$$

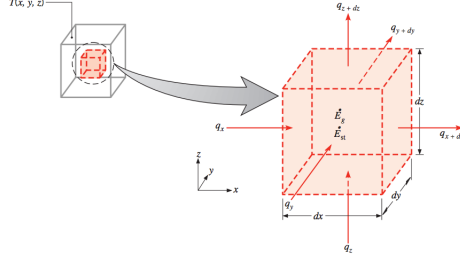


Figure 2.10: Differential control volume $dx \cdot dy \cdot dz$ in cartesian coordinates [Dewitt et al., 2007]

In the medium there may be thermal energy generation. The energy source term is expressed by

$$E_g = \dot{q} \cdot dx \cdot dy \cdot dz, \quad (2.45)$$

where \dot{q} is the energy rate which is generated per unit volume. Changes in the amount of internal energy may also occur. This energy term represents the energy stored by the material in the control volume, and may be written as

$$E_{st} = \rho c \frac{\partial T}{\partial t} dx dy dz, \quad (2.46)$$

where ρ is the density of the slab and c is its specific heat capacity. By using the fact that energy is conserved, we get the equation

$$E_{in} + E_g - E_{out} = E_{st}, \quad (2.47)$$

where

$$E_{in} = q_x + q_y + q_z, \quad (2.48)$$

and

$$E_{out} = q_{x+dx} + q_{y+dy} + q_{z+dz}. \quad (2.49)$$

By combining Eqs. 2.45, 2.46, 2.47, 2.48 and 2.49, we obtain

$$q_x dy dz + q_y dx dz + q_z dx dy + \dot{q} dx dy dz - q_{x+dx} - q_{y+dy} - q_{z+dz} = \rho c_p \frac{\partial T}{\partial t} dx dy dz. \quad (2.50)$$

Substituting Eq. 2.42, 2.43 and 2.44, we get

$$-\frac{\partial q_x}{\partial x} dx dy dz - \frac{\partial q_y}{\partial y} dx dy dz - \frac{\partial q_z}{\partial z} dx dy dz + \dot{q} dx dy dz = \rho c_p \frac{\partial T}{\partial t} dx dy dz. \quad (2.51)$$

Finally, by combining Eqs. 2.51 with Fourier's law (Eq. 2.60, 2.61 and 2.62) the heat diffusion equation is expressed as

$$\frac{\partial}{\partial x} \left(k \frac{\partial T}{\partial x} \right) + \frac{\partial}{\partial y} \left(k \frac{\partial T}{\partial y} \right) + \frac{\partial}{\partial z} \left(k \frac{\partial T}{\partial z} \right) + \dot{q} = \rho c_p \frac{\partial T}{\partial t}, \quad (2.52)$$

where ρ is the density, c_p is the specific heat capacity and \dot{q} is the rate at which energy is generated per unit volume of the medium (W/m^3). If the thermal conductivity, k , is constant, equation 2.52 can be written as

$$\frac{\partial^2 T}{\partial x^2} + \frac{\partial^2 T}{\partial y^2} + \frac{\partial^2 T}{\partial z^2} + \frac{\dot{q}}{k} = \frac{1}{\alpha} \frac{\partial T}{\partial t}. \quad (2.53)$$

The thermal diffusivity, α (m^2/s) is a measure of how quickly a material can carry heat away from a source. It can be expressed as

$$\alpha = \frac{k}{\rho c_p}. \quad (2.54)$$

2.3.4 Transient conduction

A transient or unsteady heat transfer problem is a problem with a temperature that varies with time. We have a transient heat transfer problem if a system experiences a change in operating conditions and it proceeds until a new thermal equilibrium is achieved. The changes can be induced by surface convection conditions, surface radiation conditions, internal energy generation or a change in surface temperature or heat flux. In this section I will outline a simplified model of solving certain transient problems neglecting spatial variations of temperature [Jiji, 2009].

The lumped capacitance method is the simplest approach to solving transient problems. Because the temperature gradients within the medium is considered negligible, the temperature is assumed to vary with time only, that is

$$T = T(t). \quad (2.55)$$

Under certain conditions, which will be discussed, this can be justified. Consider a hot copper wire at initial temperature T_i . It is immersed in a liquid with lower temperature, $T_{\text{inf}} < T_i$, at time $t = 0$, allowed to cool by convection heat transfer, with a heat transfer coefficient, h , at the interface between the solid and the liquid. The temperature of the wire will decrease as $t > 0$ until at some time it reaches $T = T_{\text{inf}}$ [Partlov, 2015].

However, the temperature drop, ΔT , across the radius of the metal is neglected in the lumped capacitance method. The radius of the wire r_0 , the heat transfer coefficient h , and thermal conductivity k are the factors influencing this drop [Jiji, 2009]. By dimensional analysis of the boundary conditions and governing equations a parameter that gives a measure of the temperature drop can be established by combining these three equations. The Biot number, Bi , is this parameter found to be, which is defined as

$$Bi = \frac{h\delta}{k}, \quad (2.56)$$

where δ is the length scale where the temperature drop ΔT is neglected. In this example $\delta = r_0$, but for an irregularly shaped body the length scale can be defined as the ratio of the solids volume to surface area. By comparing approximate transient solutions, results indicate that for $Bi \leq 0.1$ the temperature drop is negligible. Thus, the justification for using the lumped capacitance method is

$$Bi = \frac{h\delta}{k} \leq 0.1. \quad (2.57)$$

Consider the wire which has a surface area, A_s and a volume V . Energy will be generated volumetrically at a rate q'' (W/m^3). Assuming $Bi \leq 0.1$ we can use the lumped capacity method to determine the transient temperature. As in last section the temperature variation is governed by conservation of energy

$$\dot{E}_{in} + \dot{E}_g - \dot{E}_{out} = \dot{E}, \quad (2.58)$$

where

- \dot{E}_{in} is the rate of energy added,
- \dot{E}_g is the rate of energy generated,
- \dot{E}_{out} is the rate of energy removed,
- \dot{E} is the rate of energy change within the region.

Because heat is removed, $\dot{E}_{in} = 0$, and Eq. 2.58 becomes

$$\dot{E}_g - \dot{E}_{out} = \dot{E}. \quad (2.59)$$

If we are assuming that heat is removed by convection and neglecting radiation, Newton's law of cooling gives

$$\dot{E}_{out} = hA_s(T - T_{inf}). \quad (2.60)$$

The rate of energy generated, \dot{E}_g , is formulated by assuming that energy is uniformly generated throughout at a rate q'' per unit volume

$$\dot{E}_g = Vq''. \quad (2.61)$$

The rate of energy change within the region, \dot{E} , for incompressible material, is given by

$$\dot{E} = \rho c_p V \frac{dT}{dt}, \quad (2.62)$$

where c_p is specific heat and ρ is density. Substituting 2.60, 2.61 and 2.62 into 2.59 we get

$$Vq'' - hA_s(T - T_{inf}) = \rho c_p V \frac{dT}{dt}. \quad (2.63)$$

By separation of variables and rearranging gives

$$\frac{dT}{\left(\frac{hA_s}{q''V}\right)(T - T_{inf}) - 1} = -\frac{q''}{\rho c_p} dt. \quad (2.64)$$

This equation is the governing equation. It is valid for all bodies that generate energy volumetrically and exchange heat by convection. It is based on the assumptions that energy is uniformly generated, $Bi \leq 0.1$, radiation is negligible and the material is incompressible. For this first order differential equation, the initial condition is

$$T(0) = T_i. \quad (2.65)$$

Assuming constant h , T_∞ , and q'' and using Eqn. 2.65, direct integration of Eqn. 2.64 gives

$$\frac{T - T_\infty}{T_i - T_\infty} = \left[1 - \frac{q''V}{hA_s(T_i - T_\infty)} \right] \exp \left[-\frac{hA_s}{\rho c_p V} t \right] + \frac{q''V}{hA_s(T_i - T_\infty)}. \quad (2.66)$$

When there is no energy generation, $q'' = 0$ and 2.66 becomes

$$\frac{T - T_\infty}{T_i - T_\infty} = \exp \left[-\frac{hA_s}{\rho c_p V} t \right]. \quad (2.67)$$

If $Bi > 0.1$ spatial temperature variations must be taken into consideration. In this case, conduction is governed by a partial differential equation. For such transient problems, separation of variables can be applied to the solution. An initial condition must be specified, in addition to boundary conditions [Jiji, 2009].

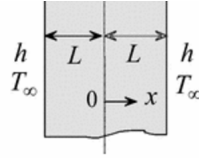


Figure 2.11: Plate with surface convection [Jiji, 2009]

In a plate of width $2L$, as in Figure 2.11 which is initially at a specified temperature given by $T_i = T(x, 0) = f(x)$, consider one-dimensional transient conduction. The ambient fluid has a temperature of T_∞ , which the plate is suddenly allowed to have convective heat transfer with. The thermal diffusivity is α and the convection coefficient is h . By defining a new temperature variable $\theta(x, t) = T(x, t) - T_\infty$, a convection boundary condition can be made homogeneous. The temperature is symmetrical about the center line, and the origin is taken at the center plane as Figure 2.11 shows. We consider constant conductivity, constant diffusivity, constant ambient temperature and constant heat transfer coefficient. Eq. 2.52 simplifies to

$$\frac{\partial^2 \theta}{\partial x^2} = \frac{1}{\alpha} \frac{\partial \theta}{\partial t}. \quad (2.68)$$

The boundary conditions at $x = 0$ and $x = L$ are respectively

$$\frac{\partial \theta(0, t)}{\partial x} = 0, \text{ and} \quad (2.69)$$

$$-k \frac{\partial \theta(L, t)}{\partial x} = h\theta(L, t). \quad (2.70)$$

The initial condition is

$$\theta(x, 0) = f(x) - T_\infty. \quad (2.71)$$

To solve this problem, separation of variables is applied. Assume a solution of the form

$$\theta(x, t) = X(x)\tau(t). \quad (2.72)$$

Substituting this into Eq. 2.68, using separation of variables and then setting the resulting equation equal to a separation constant $\pm \lambda_n^2$, we get

$$\frac{d^2 X_n}{dX^2} \pm \lambda_n^2 X_n = 0, \text{ and} \quad (2.73)$$

$$\frac{d\tau_n}{dt} \pm \alpha \lambda_n^2 \tau_n = 0. \quad (2.74)$$

The solution of Eqns. 2.73 and 2.74 are

$$X_n(x) = B_n \cos \lambda_n x. \quad (2.75)$$

The boundary condition at $x = L$ gives the characteristic equation for λ_n as

$$\lambda_n L \tan \lambda_n L = Bi. \quad (2.76)$$

Substituting into Eqn. 2.72 and summing all the solutions gives

$$\theta(x, t) = T(x, t) - T_\infty = \sum_{n=0}^{\infty} a_n \exp(-\alpha \lambda_n^2 t) \cos \lambda_n x. \quad (2.77)$$

Using the initial condition, we get

$$f(x) - t_\infty = \sum_{n=0}^{\infty} a_n \cos \lambda_n x. \quad (2.78)$$

By using orthogonality we can find a_n as

$$a_n = \frac{2\lambda_n \int_0^L [f(x) - t_\infty] \cos \lambda_n x dx}{\lambda_n L + (\sin \lambda_n L)(\cos \lambda_n L)}. \quad (2.79)$$

As seen in Figure 2.12 the temperature variation is a strong function of the Biot number and the figure shows the three different conditions where $Bi < 1$, $Bi = 1$ and $Bi > 1$. If the Biot number is small the assumption of a uniform temperature distribution is reasonable. Then the resistance to convection across the fluid boundary layer is much larger than the resistance to conduction within the solid.

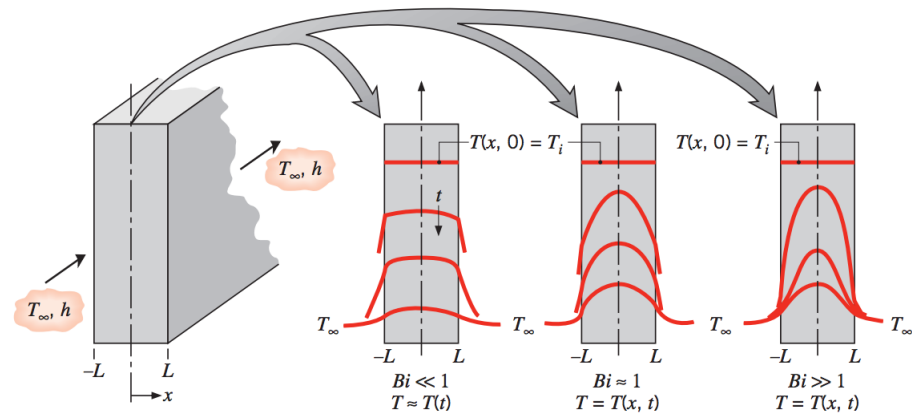


Figure 2.12: Transient temperature distributions for different Biot numbers in a plane wall symmetrically cooled by convection. [Dewitt et al., 2007]

2.3.5 Convection

Convection is a term of heat transfer taking place when we have movement of the heated parts of a gas or a liquid. Convective heat transfer includes both energy transfer due to random motion of molecules and the bulk fluid motion of the fluid [Dewitt et al., 2007]. The motion is due to the large numbers of molecules that are moving in the fluid or the gas and this movement contributes to the heat transfer. The total heat transfer is a superposition of the of the energy transport by the bulk motion and the random movement of the molecules.

In convective heat transfer the concept of boundary layers is central. When we have flow over a surface, as in Figure 2.13, the fluid particles in contact with the surface assume zero velocity. These particles will act to retard the motion of particles in the next layer, and so on, until a distance from the surface where this effect is negligible and we have free stream. This effect is associated with shear stresses parallel to the velocity of the fluid. The x velocity component of the fluid, u , will increase with increasing distance y from the surface until it approaches free stream, u_∞ . The thickness of the velocity boundary layer is typically defined as the value of y , for which $u = 0.99u_\infty$. The boundary layer velocity profile is the change in the velocity with distance from the surface through the boundary layer [Dewitt et al., 2007].

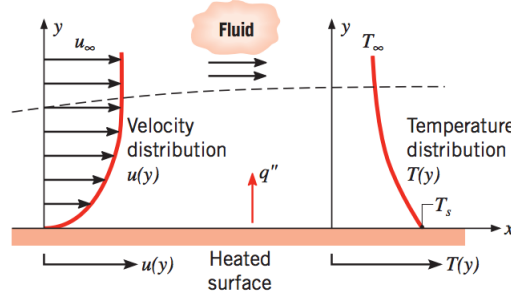


Figure 2.13: Development of boundary layer in convective heat transfer [Zhang et al., 2008]

If the temperature of the surface and the fluid free stream differ a thermal boundary layer will develop. Consider a heated surface with temperature T_s as in Figure 2.13 and a surrounding fluid with temperature T_∞ . The fluid particles in contact with the bounding surface achieves thermal equilibrium with the surface temperature. These particles, in turn, exchange energy with particles in the next fluid layer and temperature gradients will develop in the fluid. A thermal boundary layer will develop in the region with these temperature gradients and its thickness is usually defined as the value of y for which the ratio $[(T_s - T)/(T_s - T_\infty)] = 0.99$.

The boundary layer can be laminar or turbulent, or in many cases both conditions occur. The fluid flow is highly ordered in the laminar boundary layer and it is possible to identify streamlines. In the turbulent boundary layer, the flow is irregular with a random motion. Whether the boundary layer is laminar or turbulent are strongly depending the convection transfer rate and surface friction.

We can also both have natural and forced convection. In natural convection the flow is induced by buoyancy forces, which are due to differences in density caused by variations in composition and/or temperature. Forced convection is caused by external means in the flow, such as by a pump or a fan.

The convection heat transfer rate equation can be written as

$$q_s = h(T_s - T_\infty), \quad (2.80)$$

where h ($\text{W}/\text{m}^2\text{K}$) is the convection heat transfer coefficient. The quantity, q_s (W/m^2), is the convective heat flux and it is proportional to the difference between the temperature of the surface, T_s , and the fluid T_∞ .

2.3.6 Radiation

The process in which energy is emitted by a heated surface is called thermal radiation. The emission is related to energy released when we have transitions or oscillations of the constituent electrons [Dewitt et al., 2007].

Emission from a solid or a liquid can be viewed as a surface phenomenon, because the emitted radiation originates from molecules in a distance of approximately $1 \mu\text{m}$ from the surface that is exposed. Radiation can propagate in all possible directions, and to quantify this radiation emission, both the spectral distribution and the directional distribution must be treated [Dewitt et al., 2007].

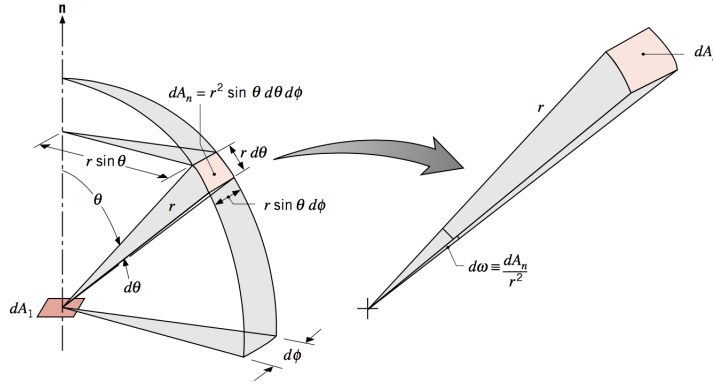


Figure 2.14: Emission of radiation in a spherical coordinate system [Dewitt et al., 2007]

By introducing the concept of radiation intensity, the directional effects may be considered. Shown in Figure 2.14, the emission of radiation from a differential area dA_1 , into a solid angle, $d\omega$ may be subtended by an area dA_n at a point on dA_1 . The angle $d\omega$ is defined as

$$d\omega \equiv \frac{dA_n}{r^2} = \sin \theta d\theta d\phi, \quad (2.81)$$

where r is the radius of the circle.

From Figure 2.14, we define $I_{\lambda,e}$ as the rate at which radiant energy is emitted from dA_1 that passes through dA_n at the wavelength λ in the (θ, ϕ) direction, per unit solid angle about this direction, per unit area of the emitting surface normal to this direction and per unit wavelength interval $d\lambda$ about λ . This quantity is called the spectral intensity and may be expressed as

$$I_{\lambda,e}(\lambda, \theta, \phi) = \frac{dq}{dA_1 \cos \theta \cdot d\omega \cdot d\lambda}, \quad (2.82)$$

where $dq_\lambda = \frac{dq}{d\lambda}$ is the rate at which radiation leaves dA_1 and passes through dA_n with a wavelength λ .

Radiation may also be related to irradiation and radiosity. Irradiation, G , represents the rate at which radiant energy is incident from all directions and at all wavelengths, per unit area, and may be expressed as

$$G = \int_0^\infty \int_0^{2\pi} \int_0^{\frac{\pi}{2}} I_{\lambda,i}(\lambda, \theta, \phi) \cos \theta \sin \theta d\theta d\phi d\lambda, \quad (2.83)$$

where $I_{\lambda,i}$ represents the spectral intensity of incident radiation.

Radiosity accounts for all the radiation leaving a surface and can be written as

$$J = \int_0^\infty \int_0^{2\pi} \int_0^{\frac{\pi}{2}} I_{\lambda,e+r}(\lambda, \theta, \phi) \cos \theta \sin \theta d\theta d\phi d\lambda. \quad (2.84)$$

If the surface is both a diffuse emitter and reflector, $I_{\lambda,e+r}$ is independent of θ and ϕ , and the radiosity can be written as

$$J = \pi I_{e+r}. \quad (2.85)$$

When we have a real surface instead of ideal or "black" surface behavior, a radiative property called the emissivity is considered. The spectral, directional emissivity $\epsilon_{\lambda,\theta}(\lambda, \theta, \phi, T)$ of a surface with a temperature T is defined as the ratio of the emitted radiation intensity at the wavelength λ , in the direction of θ and ϕ to the intensity of the emitted radiation of an ideal surface at the same temperature and wavelength.

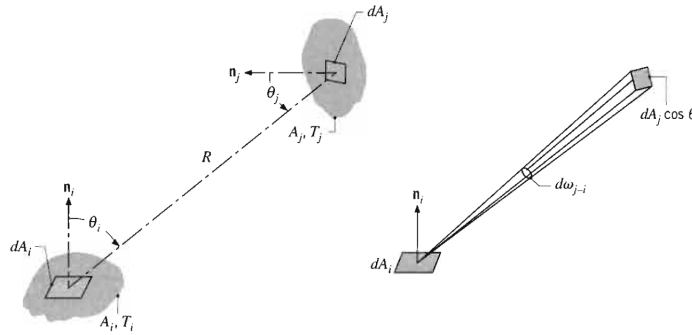


Figure 2.15: The view factor associated with the radiation exchange between the surfaces A_i and A_j [Dewitt et al., 2007]

When we have radiation exchange between surfaces it depends on the radiative properties, as well as surface geometries and orientations. To compute this radiation exchange, the concept of a view factor is used. The fraction of the

radiation leaving the surface i and is intercepted by surface j is defined as the view factor, F_{ij} [Dewitt et al., 2007].

In Figure 2.15 we have two surfaces A_i and A_j , which is arbitrarily oriented. From Eqn. 2.82, the rate at which radiation leaves dA_i and is intercepted by dA_j can be written as

$$dq_{i \rightarrow j} = I_{e+r,i} \cos \theta_i dA_i d\omega_{j-i}, \quad (2.86)$$

where $d\omega_{j-i}$ is the solid angle subtended by dA_j , viewed from dA_i . $I_{e+r,i}$ is the radiation intensity leaving surface i and $d\omega_{j-i}$. With Eqn. 2.81 it follows that

$$dq_{i \rightarrow j} = I_{e+r,i} \frac{\cos \theta_i \cos \theta_j}{R^2} dA_i dA_j. \quad (2.87)$$

Substituting from Eqn. 2.85, assuming that surface i is emitting and reflecting diffusely and integrating over the two surfaces, we get

$$q_{i \rightarrow j} = J_i \int_{A_i} \int_{A_j} \frac{\cos \theta_i \cos \theta_j}{\pi R^2} dA_i dA_j. \quad (2.88)$$

Because the view factor, F_{ij} , is defined as the fraction of the radiation from A_i and is intercepted by A_j , we get

$$F_{ij} = \frac{1}{A_i} \int_{A_i} \int_{A_j} \frac{\cos \theta_i \cos \theta_j}{\pi R^2} dA_i dA_j. \quad (2.89)$$

The net rate of radiation from surface i , related to radiation transfer from the other surfaces can be written as

$$q_i = A_i(J_i - G_i). \quad (2.90)$$

From the definition of the view factor, the total rate of radiation energy that reaches surface i is

$$A_i G_i = \sum_{j=1}^N A_i F_{ji} J_j. \quad (2.91)$$

Using Eqns. 2.90 and 2.91, and the summation rule, q_i can be written as

$$q_i = \sum_{j=1}^N A_i F_{ij} (J_i - J_j). \quad (2.92)$$

2.3.7 Thermal resistance

Thermal resistance is defined as the potential of the driving temperature divided by heat transfer rate [Dewitt et al., 2007], and can be expressed as

$$q = \frac{\Delta T}{A \cdot R_t}, \quad (2.93)$$

where R_t is thermal resistance, A is the surface area over which the heat transfer occurs and ΔT is the relevant temperature difference.

The heat transfer for conduction, convection and radiation can also be expressed in the form of thermal resistance in the following way

$$R_{t,\text{cond}} = \frac{L}{k \cdot A}, \quad (2.94)$$

$$R_{t,\text{conv}} = \frac{1}{h \cdot A}, \quad (2.95)$$

$$R_{t,\text{rad}} = \frac{1}{h_r \cdot A}. \quad (2.96)$$

The radiation heat transfer coefficient, h_r , can be expressed as

$$h_r = \epsilon \sigma (T_s + T_{\text{sur}})(T_s^2 + T_{\text{sur}}^2). \quad (2.97)$$

2.3.8 Thermal contact resistance

At the interface of two solid surfaces pressed together, the thermal contact will not be perfect. Some roughness is always present, and tiny air gaps will often occur. Figure 2.16 shows a model of how the contact area can look like. In such an interface there will be conduction heat transfer through both the gas-filled space and through the contact points between the solids. The conduction rate through the gas-filled interstices is often poor because a gas has lower thermal conductivity than a solid. Also heat transfer through the gaps by radiation may occur if the temperatures of the surfaces are different [Lienhard, 2013].

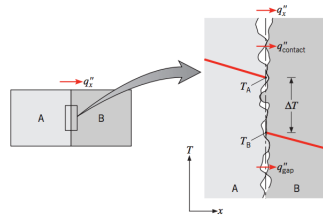


Figure 2.16: Heat transfer between two solid surfaces [Lienhard, 2013]

The interfacial conductance depends on many factors. The surface finish of the contacting solids and cleanliness are important. Also, the materials in contact, the pressure in which the materials are forced together and the temperature at the contact area matter of the thermal contact resistance.

There will be a temperature drop across the interface, as shown in Figure 2.17. Because many of the factors often are uncertain, this drop may be hard

to calculate, and so the temperature distribution. However, this drop may in some cases be appreciable.

The thermal resistance, R_t (K/W) can be expressed as

$$R_t = \frac{T_A - T_B}{A \cdot q_x}. \quad (2.98)$$

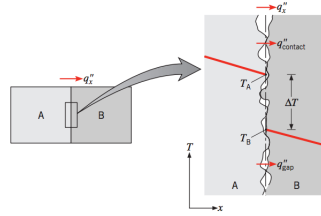


Figure 2.17: Temperature drop due to thermal contact resistance [Lienhard, 2013]

There are many ways to reduce the contact resistance. The area of the contact spots can be increased by reducing the roughness of the contacting materials and/or increasing the pressure between them. Selecting an interfacial fluid of large thermal conductivity, like soft metals will also reduce the contact resistance. Even though some theories can predict the thermal resistance, the most reliable results have been obtained by experiments [Dewitt et al., 2007].

2.3.9 Boundary and initial conditions

To solve a differential equation like the heat diffusion equation we need to specify the domain for the equation. Also because a differential equation have infinitely many solutions, we have to determine the boundary conditions and the initial condition to find a unique solution. We can have several types of boundary conditions:

1. Dirichlet condition specifies the value of the function on a boundary surface,

$$T(0, t) = T_s. \quad (2.99)$$

2. Neumann condition specifies the normal derivative of the function on a boundary surface.

We can either have a finite heat flux

$$-k \frac{\partial T}{\partial x} \Big|_{x=0} = q_s, \quad (2.100)$$

or we can have an adiabatic surface

$$\frac{\partial T}{\partial x} \Big|_{x=0} = 0. \quad (2.101)$$

3. The third boundary condition corresponds to the existence of convection at the surface

$$-k \frac{\partial T}{\partial x} \Big|_{x=0} = h[T_\infty - T(0, t)]. \quad (2.102)$$

2.3.10 Cooling methods

Heat exchangers, which is used to transfer heat between to fluids or a fluid and a solid object, have several engineering and industrial applications. The heat transfer augmentation methods can be classified into three broad categories, passive, active and compound heat transfer, where compound heat transfer is a combination of the two other methods [Liu and Sakr, 2013].

Active heat transfer involves input of external energy [Dewan et al., 2004]. In several applications, external power may not be easy to provide. Examples of active heat transfer methods are the use of fans, magnetic field and induced pulsation by cams.

When using fans, the idea is to increase the convection rate when air around the transducer is forced to move faster [Léal et al., 2013]. Air in contact with a warmer object experiences an increase in temperature. It will be lighter than the surrounding air, because of the lower density. Warm air is replaced by cooler ambient air in a vertical motion induced by buoyancy forces. This is a slow process, but with fans it will go faster. Fans can either be used to suck cool air inward or blow hot air outward.

Passive methods generally uses geometrical or surface modifications to enhance heat transfer. It does not need any external power input, and if additional power is needed it is taken from the available power in the system [Dewan et al., 2004]. One way to enhance passive heat transfer is to increase the surface area of the heat exchange. This can be done by the use of a heat sink. The heat transfer coefficient can be improved by modifying the physical properties of the surface and/or the fluid [Léal et al., 2013]. Some examples of this effect are surface coating, swirl flow devices and tension devices.

The use of heat sinks are based on the principle to dissipate heat generated by a mechanical or electronic device [Knight et al., 1991]. The heat sink is often designed with a large surface area in contact with the cooling medium surrounding it and consists of a material with high thermal conductivity. A thermal compound between the device and the heat sink may be used to fill any air gaps and optimize the heat transfer. This compound is normally called a

thermal paste or gel.

Aluminum and copper are currently the most common used materials for heat sinks [Ashby and Lu, 2003]. Aluminum has relatively high thermal conductivity, is cheap and light. Copper has higher thermal conductivity, but is heavier and more expensive. Both materials have a good resistance for corrosion.

The Peltier effect is a heat sink phenomenon that arises when applying an electric current at the junction of dissimilar materials. It is used to abstract or generate heat [Hubert, 1972]. Because the cooling effect produced is directly proportional to the supplied current, it is convenient to control cooling by adjusting the current in the circuit.

3. Simulation tool

In the simulations of the heat transfer in the multifrequency ultrasound transducer, I have used the program Comsol Multiphysics, version 5.2a, which is a finite element analysis software [Comsol, 2016]. Due to the complexity of the transducer system, numerical methods are expected to provide a complete and realistic model of the heat transfer. Comsol Multiphysics can be used to model and analyze mechanical, electrical and fluid flow in addition to a wide variety of engineering and industrial problems. In a software like this the purpose is to reduce the number of experiments and prototypes that have to be run when optimizing or designing a process [Comsol, 2016]. The laws of physics, which the software is formed by, are expressed in mathematical models.

3.1 The finite element method

Partial differential equations (PDEs) are often used to describe the laws of physics for space- and time-dependent problems. Most of these PDEs can not be solved by analytical methods. An approximation of the equations is made with different types of discretizations, and by using numerical methods it can be solved. The finite element method is a numerical technique for obtaining approximate solutions to problems described by these PDEs. The solution is then a pointwise approximation to the governing equations. [Huebner et al., 2001].

The finite element method offers great freedom in the selection of discretization and this is one of the main benefits of using this method. It envisions the solution region as built up of interconnected, small elements. These elements can be put together in many different ways, and therefore they can be used to represent complex shapes. The finite difference scheme, which is another well used numerical technique, is hard to use when we are dealing with irregular geometries or boundary conditions which has an unusual specification [Huebner et al., 2001]. Figure 3.1 shows the different meshes of a turbine blade profile for the two methods. This demonstrates that the finite element method is more suited for complex geometries problems, but it is not better for all problems.

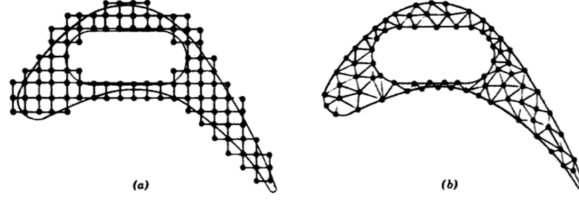


Figure 3.1: Finite difference (a) and finite element scheme (b) of a turbine blade profile [Huebner et al., 2001]

Another benefit of the finite element method is that it is well developed. This is due to the close relationship between the numerical formulation and the weak formulation of the PDE. When the model equations are solved in the analysis the method provides useful error estimates [Comsol, 2016].

3.1.1 Ordinary and partial differential equations

The conservation laws can all be expressed as PDEs. As an example of a differential equation we can have a solid with a temperature variation in time and negligible variations in space. The conservation of energy equation results in an equation for the temperature change in time due to a heat source, j

$$\rho c \frac{dT}{dt} = j(T, t). \quad (3.1)$$

In Equation 3.1, ρ is the density and c is the specific heat capacity. The heat source varies with the dependent variable temperature, T , and time t , which is the independent variable. Because we have a differential equation expressed in terms of the derivatives of one independent variable, time, this equation is an ordinary differential equation (ODE).

When we have variations in time and space, the equation of conservation of energy can be written as

$$\rho c \frac{dT}{dt} + \nabla \cdot \mathbf{q} = j(T, t, \mathbf{x}). \quad (3.2)$$

This equation expresses the changes in space, $\mathbf{x} = (x, y, z)$ and time, t , which are both independent variables. In a Cartesian coordinate system, the divergence of $\mathbf{q} = (q_x, q_y, q_z)$, the heat flux vector, can be written as

$$\nabla \cdot \mathbf{q} = \frac{\partial q_x}{\partial x} + \frac{\partial q_y}{\partial y} + \frac{\partial q_z}{\partial z}. \quad (3.3)$$

Equation 3.3 describes the change in heat flux along the spatial coordinates. By Fourier's law we can describe the heat flux in a solid as

$$\mathbf{q} = -k\nabla T \Rightarrow \mathbf{q} = \left(-k \frac{\partial T}{\partial x}, -k \frac{\partial T}{\partial y}, -k \frac{\partial T}{\partial z}\right). \quad (3.4)$$

When the thermal conductivity, k , is constant, the heat flux is proportional to the temperature gradient as Equation 3.4 shows. This equation can then be written as

$$\rho c \frac{dT}{dt} + \nabla \cdot (-k\nabla T) = j(T, t, \mathbf{x}). \quad (3.5)$$

Equation 3.5 is expressed in terms of the derivatives of more than one independent variable and is therefore a PDE. The independent variables are x, y, z and t .

If the conductivity is anisotropic, it can be described by a tensor

$$\mathbf{k} = \begin{bmatrix} k_{xx} & k_{xy} & k_{xz} \\ k_{yx} & k_{yy} & k_{yz} \\ k_{zx} & k_{zy} & k_{zz} \end{bmatrix}.$$

3.1.2 Basic functions and test functions

To describe the finite element method, assume we are studying the temperature distribution in a heat sink. If we have a steady state situation, meaning the temperature does not change with time, Equation 3.5 can be written as

$$\nabla(-k\nabla T) = j(T, \mathbf{x}) \quad \text{in } \Omega, \quad (3.6)$$

where Ω represents the domain.

I am assuming the temperature along the boundary, $\partial\Omega_1$, and the heat flux normal to some other boundary, $\partial\Omega_2$, to be known. The heat flux in the outward direction, $\partial\Omega_3$, is zero. We then have the following boundary conditions in this example

$$T = T_0 \quad \text{on } \partial\Omega_1, \quad (3.7)$$

$$(-k\nabla T) \cdot \mathbf{n} = h(T - T_{amb}) \quad \text{on } \partial\Omega_2, \quad (3.8)$$

$$(-k\nabla T)\mathbf{n} = 0 \quad \text{on } \partial\Omega_3, \quad (3.9)$$

where \mathbf{n} describes the unit normal vector pointing outwards from the boundary surface, T_{amb} is the ambient temperature and h is the heat transfer coefficient.

Multiplying with a test function, ϕ , and then integrating, we get

$$\int_{\Omega} \nabla \cdot (-k\nabla T) \phi \, dV = \int_{\Omega} g \phi \, dV. \quad (3.10)$$

We then get a function space, called a Hilbert space, with the same properties as ordinary vectors in a vector space. In a Hilbert space the length and angle between the functions can be measured.

After converting the functions in an infinite dimensional function space, with the finite element method, to ordinary vectors, we can use numerical methods to solve the functions.

Using integration by parts, we are obtaining the weak form as

$$\int_{\Omega} k \nabla T \cdot \nabla \phi \, dV + \int_{\partial\Omega} (-k \nabla T) \cdot \mathbf{n} \phi \, dS = \int_{\Omega} g \phi \, dV. \quad (3.11)$$

By discretization of the mathematical model equations we can obtain the numerical model equations. When we are discretizing, we approximate the solution of Eqn. 3.11, which should be in the subspace of the Hilbert space, H , so that $T \approx T_H$. The approximated solution, $T_H(x)$, can be expressed as a linear combination of a set of basic functions, ϕ_i , in the subspace

$$T_H(\mathbf{x}) = \sum_i T_i \phi_i(\mathbf{x}). \quad (3.12)$$

When the boundary conditions are used and the system is discretized, Eq. 3.11 together with Eq. 3.12 can be written as a system of equations

$$\mathbf{A} \mathbf{T}_H = \mathbf{b} \quad (3.13)$$

The column vectors, \mathbf{T}_H and \mathbf{b} , have n entries of unknown temperatures, while \mathbf{A} is a $n \times n$ matrix. The solution of this system of equations is then the approximated solution to the PDE.

We need to discretize the time derivative if also the temperature is varying with time. We can do this with finite differences, obtaining

$$\frac{\partial T_i}{\partial t} \approx \frac{T_{i,t+\Delta t} - T_{i,t}}{\Delta t}. \quad (3.14)$$

The system of equations can then be solved with one equation for each time step.

3.1.3 Finite element mesh refinement

After modelling the geometry and knowing the physics and the material properties relevant to the problem, the model has to be divided into smaller elements. A set of equations are solved over each element. Smaller elements will make the computed solution closer and closer to the true solution. The accuracy is related directly to the mesh that is used.

In the analysis process, it is often a good idea to start with a mesh with large elements, a preliminary mesh. It may give an inaccurate solution, but the solution requires less computational resources, and it can be used as a check on the applied constraints and as a rough verification.

The mesh is refined when these elements are made successively smaller and smaller later in the process. When comparing the results between these different meshes, we can judge the convergence of the solution. We consider the model to be converged when the changes in the solution becomes small enough. This call is always a judgement call with respect to the uncertainties in the model input and the acceptable uncertainty in the results.

3.1.4 Mathematical model and numerical model

A systems mathematical model can consist of one or several PDEs together with initial and boundary conditions. The boundary conditions has to be satisfied at all or part of the modeled domain. The initial conditions are a set of starting-point values of the system.

A mathematical model has to be properly defined to get a solution. Being well-posed means that the model has a unique solution continuously depending on the problem data. To see if a problem is well-posed can be difficult, and in fundamental analysis greatly simplified models are often used.

The numerical methods are often based on a discretization of the model domain and the dependent variables described. Finite element, finite volume and finite differences methods are most commonly used for the discretization. The models can then give an approximation of the solution to a mathematical model that is well posed.

3.1.5 Errors in finite element analysis

Because of some errors the finite element simulations will differ from their exact values. The error due to the representation of a function or a continuous equation in a discrete domain of space is called the discretization or the truncation error. When letting the grid space go to zero the discretization error is usually reduced.

Because the iterative method may eventually have a stopping point, we have a convergence error . To define a stopping criteria, we need to calculate the difference between the iterate solution and the true solution, and this difference is called the convergence error.

We also have some errors due to simplifications and uncertainty in the formulation of the model, and computer round-off errors which develop with the representation of floating point numbers on the computer. This errors are called physical modelling errors.

3.2 Transport phenomena

Heat transfer, fluid flow and mass transfer are examples of transport phenomena. The physical relations describing these phenomena are based on the conservation laws of momentum, mass, and energy. Differential equations are used to describe these laws of conservation.

3.2.1 Conservation of energy

The basis for the transport of momentum, energy and mass are the conservation laws, which can be derived from simple principles. To show how energy is conserved, I am going to consider a tiny volume element in a continuum, shown in figure 3.2. According to the energy balance, any production or consumption of energy, S , in the volume element, Δx , Δy , and Δz , must be caused by the energy flux, j , into or out of the volume element,

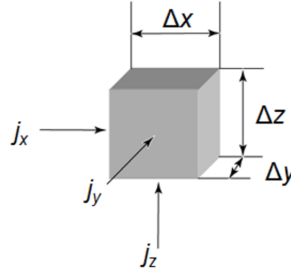


Figure 3.2: A small volume element with dimensions Δx , Δy , and Δz . The flux, $j = (j_x, j_y, j_z)$, is given in quantity per unit area and unit time [Comsol, 2016]

$$\begin{aligned} \Delta x \Delta y \Delta z \frac{\phi_{t+\Delta t} - \phi_t}{\Delta t} = & -(\Delta y \Delta z (j_{x,x+\Delta x} - j_{x,x}) + \Delta x \Delta z (j_{y,y+\Delta y} - j_{y,y}) \\ & + \Delta x \Delta y (j_{z,z+\Delta z} - j_{z,z})) + \Delta x \Delta y \Delta z S \end{aligned} \quad (3.15)$$

The quantity ϕ is conserved in the system, and Eq. 3.15 shows the balance of this quantity. If we divide Eq. 3.15 by $\Delta x \Delta y \Delta z$ and letting Δx , Δy , Δz and Δt go to zero, we obtain

$$\frac{\partial \phi}{\partial t} = - \left[\frac{\partial j_x}{\partial x} + \frac{\partial j_y}{\partial y} + \frac{\partial j_z}{\partial z} \right] + S. \quad (3.16)$$

This differential equation has to be satisfied in every volume element in the continuum. By solving this equation under different conditions, we can see how the energy is transferred in the system. For transient simulations, the spatial integral is evaluated at each time step.

3.2.2 Tolerances for a time dependent problem

The relative tolerance and absolute tolerance are used by Comsol Multiphysics as convergence criteria in the time-stepping algorithms. The default value of relative tolerance (R) is 0.01, and for the absolute tolerance (A_i) it is 0.001. The step is accepted if

$$\left[\frac{1}{N} \sum_i \left(\frac{|E_i|}{A_i + R|U_i|} \right)^2 \right]^{\frac{1}{2}} < 1, \quad (3.17)$$

where U is the solution vector at a certain time step, E is the error in U during this time step, estimated by the solver and N is the number of degree of freedom.

4. Thermal design: development and analysis

The problem to be solved is modelling the heat transfer in the transducer due to acoustic energy absorption. With the program x-trans the heat sources are calculated. The heat equations which describe the thermal energy generation are simulated in Comsol.

The heat transfer is considered uniform within the different layers of the transducer and that the heat is passively spread out to the external transducer surface area. Between the layers we may have a temperature drop because of thermal contact resistance. It may be dominating when we have good heat conductors like copper. Piezoelectric ceramic and epoxy on the other side have low thermal conductivity and these layers make the heat loss less dominating in the transducer. Also the surface finish of the contacting solids is smooth so I am neglecting the thermal contact resistance in the simulations.

The heat transfer can be divided into two parts. The first part treats the conductive heat transfer inside the transducer, and the second part deals with the heat transfer from the transducer to the surroundings. The geometry and heat generation of the transducer will be step-wise described and analyzed in the following sections. To begin with, a design of the transducer used today will be presented, along with the materials used. Then, some different transducer geometries will be studied. All the elements and conditions required for the analysis will be implemented and analyzed. At the end, methods to cool the transducer will be presented and simulated.

4.1 Geometry

Figure 4.1 shows the geometry of the multifrequency ultrasound transducer used today in the yz-plane. The width is 34.56 mm (x-axis) and the length is 5 mm (y-axis). The height is denoted in the z-dimension. In the figure, point (0,0,0) is at the bottom left corner of the transducer.

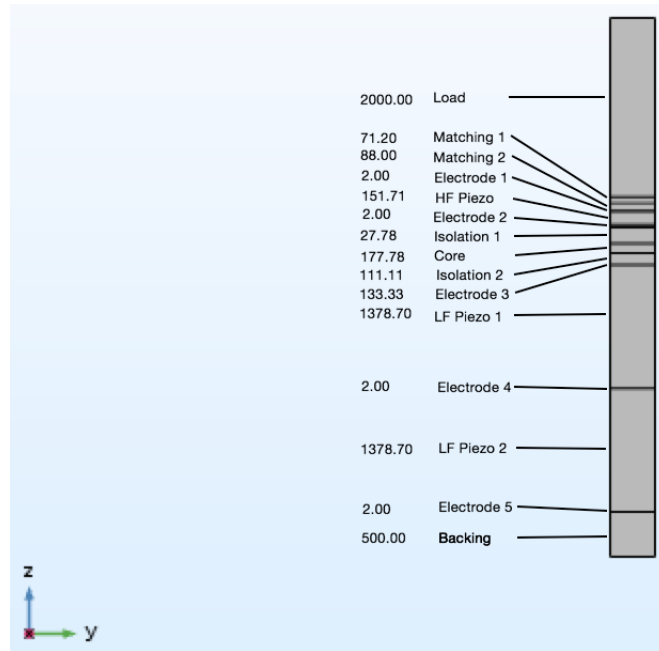


Figure 4.1: Design of the transducer stack, showing the thickness of each layer in μm .

The multifrequency transducer in this simulation has two LF layers, one HF layer as Figure 4.1 shows. The HF layer is the piezoelectric layer closest to the load and it is used to transmit and receive waves at high frequencies. The LF layers transmit waves at low frequencies and are coupled together in parallel with a signal electrode in between. More about how the transducer works are described in Section 2.1.3. The load is the body of the patient.

4.2 Materials

We have three groups of materials in the transducer stack. These are copper, epoxy and ceramic. In the simulation we also have the biological material the transducer is placed on which is called the load.

4.2.1 Copper

For the electrodes, the backing and the core, copper is used. Comsol has a material library, which represent some materials by referenced property functions.

The material parameters of copper at 298 K are:

- Density: 8960 kg/m³
- Specific heat capacity: 385 J/(kgK)
- Thermal conductivity: 400 W/(mK)

As Figure 2.8 shows, the thermal conductivity of copper does not vary much with temperature.

4.2.2 Epoxy

Epoxy is the material used for the matching and isolation layers. Epoxy may refer to a broad range of polymer materials, but in the transducer, epoxy layers with acoustic properties have been designed to achieve optimum matching of the transducer to the load.

The parameters of this material at 298 K are:

- Density: 1250 kg/m³
- Specific heat capacity: 2100 J/(kgK)
- Thermal conductivity: 0.2-1.7 W/(mK)

In the transducer, epoxy with "Ugelstad"-spheres are going to be used. Ugelstad spheres are monodispersed magnetizable particles which have found application in liquid chromatography among others [Ugelstad et al., 1985]. The spheres used in the epoxy layer are tiny biomagnetic spheres covered with a metallic layer. This is to optimize the properties for the transducer used in ultrasound therapy. They are made by a company called Conpart and the thermal conductivity of layers with Ugelstad spheres is shown in Figure 4.2.

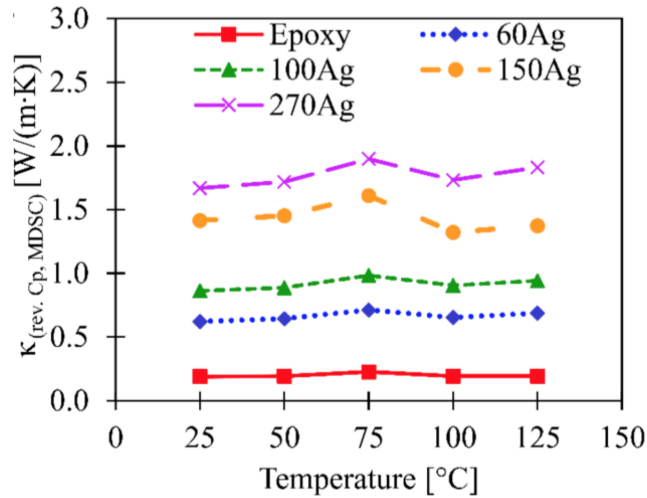


Figure 4.2: Thermal conductivity of layers with "Ugelstad"-spheres depending on temperature and thickness of the silver coating, tested by Conpart. The silver coating thickness of the spheres are described in nanometres.

In the matching and isolation layers, spheres with a diameter of $30 \cdot 10^{-6}$ m are used. The volume percent of the spheres to epoxy is 50. As Figure 4.2 shows, the thermal conductivity of epoxy does not depend much with temperature, and for the simulations I will use a thermal conductivity of 0.2 W/(mK) .

4.2.3 Piezoelectric ceramic

Generally, a piezoelectric ceramic is a material that either exhibit a dimensional change or output a voltage when subjected to a mechanical stress when an electric field is applied [Hooker, 1998]. The piezoelectric material in a transducer converts electrical energy into mechanical vibrations as described in Section 2.1.3. An example of a piezoelectric ceramic is lead zirconate titanate (PZT). It has a high electromechanical coupling coefficient and a low acoustic impedance. It is often used for the piezoelectric layer in an ultrasound transducer [He, 2004].

Comsol specifies the material properties of lead zirconate titanate (PZT-5H) at 298 K as:

- Density: 7500 kg/m^3
- Specific heat capacity: 420 J/(kgK)
- Thermal conductivity: 1.8 W/(mK)

Load

The load consists of skin, tissue and biological fluids. Average physical properties for the load are:

- Density: 1000 kg/m^3
- Specific heat capacity: 3700 J/(kgK)
- Thermal conductivity: 0.21 W/(mK)

[Poppendiek et al., 1967] [Duck, 2013] [Giering et al., 1996]

4.3 Domain settings, boundary conditions and initial conditions

As described in Section 2.3.5 and 2.3.6 the boundary conditions we have to consider are natural convection and radiation between the device and the surroundings. The transducer is used in an environment with air as the surrounding fluid. The initial temperature was set as room temperature, 298 K, and with an initial pressure of 1 bar. The boundary condition for the load is convective heat transfer to tissue with a temperature of 310 K. The physical properties of air and tissue are described in Table 4.1.

Table 4.1: The properties of air at a pressure of 1 bar and 298 K, specified by Comsol and the properties of tissue as described in Section 4.2.4

	ρ [kg/m ³]	C_p [kJ/(kg · K)]	k [W/(m · K)]
Air	1.1832	1.007	26.1*10 ⁻³
Tissue	1000	3.7	0.21

The transducer may be exposed to radiation, which can be significant, emitted by lighting and other electrical devices. Typically, the transducer has a plastic cover and is used in a normal indoor environment which can be considered as radiation exchange in an enclosure. Radiation may experience multiple reflections off all surfaces with partial absorption occurring at each.

By making certain assumptions the situation can be simplified. Each surface is assumed isothermal and to be characterized by a uniform radiosity and a uniform irradiation. Also, assuming negligible differences in temperature between heat-emitting surfaces, it can be considered that there is no radiation net heat exchange with the transducer [Sadrizadeh and Holmberg, 2015] [Mangum and Hill, 1977]. I am therefore neglecting the thermal radiation in the simulations and will only consider convection.

Then, as described in Section 2.3.9, the boundary condition corresponds to the existence of convection at the surface, and can be written as

$$-k \frac{\partial T}{\partial x} \Big|_{x=0} = h[T_\infty - T(0, t)], \quad (4.1)$$

$$Q_{\text{tot}} = Q_{\text{conv}}, \quad (4.2)$$

$$R_{\text{tot}} = R_{\text{conv}}. \quad (4.3)$$

The total heat transfer and thermal resistance from the transducer casing and the surroundings is shown in Figure 4.3.

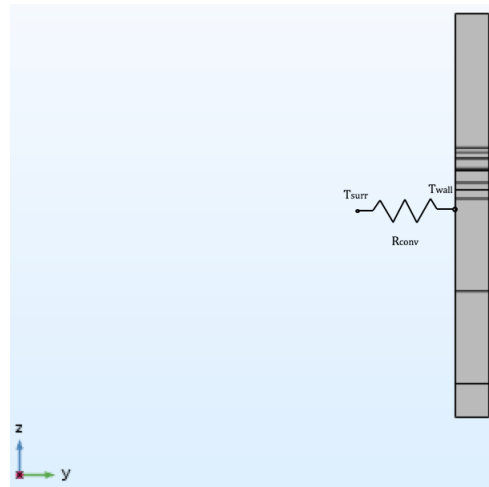


Figure 4.3: Thermal resistance between the transducer and the surrounding fluid

4.4 Mesh

When doing numerical simulations, the model has to be divided into a finite element mesh. The mesh divides both subdomains into elements and boundaries into boundary elements [Comsol, 2016]. In the transducer, the domain is not very complex or with extreme aspect ratios and the geometry will mesh with the default settings. The mesh quality is selected normal, and only the parameters in the custom mesh have to be determined.

4.5 Simulation setup

4.5.1 Heat generation

When the electric energy is converted into useful acoustic energy in the piezoelements, energy is also converted to thermal energy as described in Section 2.2. This energy conversion takes place at the boundaries between the backing material, matching layers, the core and the isolation layers in the transducer. To measure these heat sources the program x-trans, which is a 1D simulation program used to optimize the acoustic design of transducers, is used. In cooperation with my supervisors, we are studying the analysis of vibrations and modifying the equations to produce spatially distributed heat sources in the different layers.

Because of the periodic acoustic waves the heat sources are defined periodically. From x-trans we found that the heat sources are applied for $1.025 \cdot 10^{-9}$ s and this is repeated every 1/15000 s in the layers.

4.5.2 Heat development

When simulating the temperature distribution in the transducer we are first going to measure where the warmest point is located. Then, we are going to simulate the transducer for 10 seconds as an arbitrary value to start with. This is to decide if we can consider the temperature development as steady state or do any other simplifications for the simulations.

In cooperation with my supervisors, we have decided three different structures to investigate to see how the material and geometry affects the temperature distribution.

- The first geometry is shown in Figure 4.4. This is the whole transducer as described in Section 4.1.

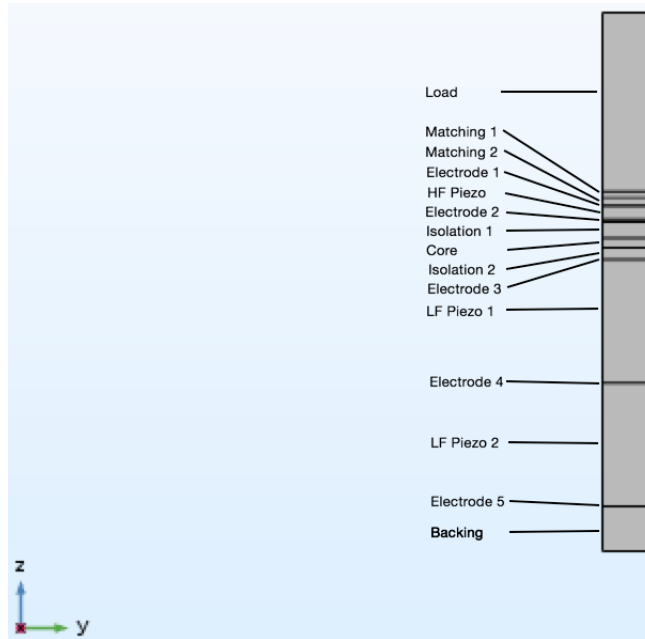


Figure 4.4: Transducer Geometry 1

- Figure 4.5 shows the second geometry. In this geometry we have the matching 1, matching 2, electrode 5, HF piezo and the backing layer. The thickness of the layers are the same as in Geometry 1, except for the backing layer which is thicker. The total height for the two geometries are the same.

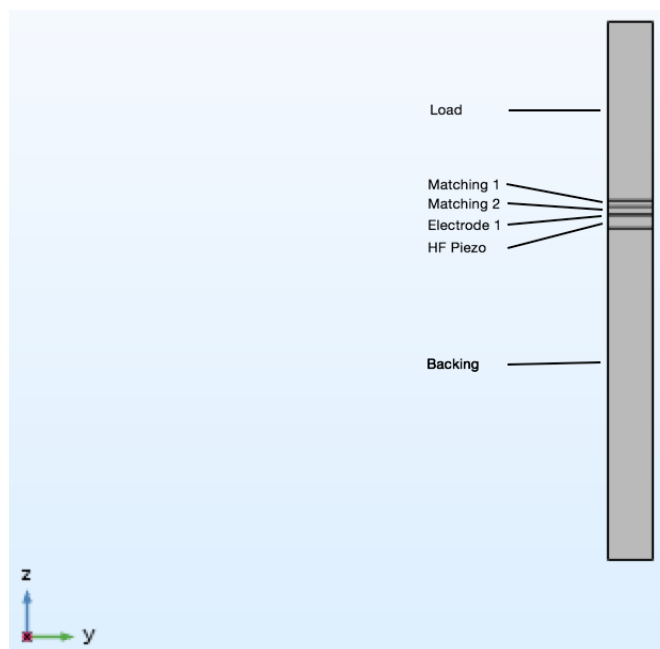


Figure 4.5: Transducer Geometry 2

- The third geometry is shown in Figure 4.6. This geometry includes the matching 1, matching 2, electrode 5 and the backing layer. As in Geometry 2, the thickness of all the layers, except for the backing layer, are the same as in Geometry 1. The backing layer is thicker making the total height for the geometries the same.

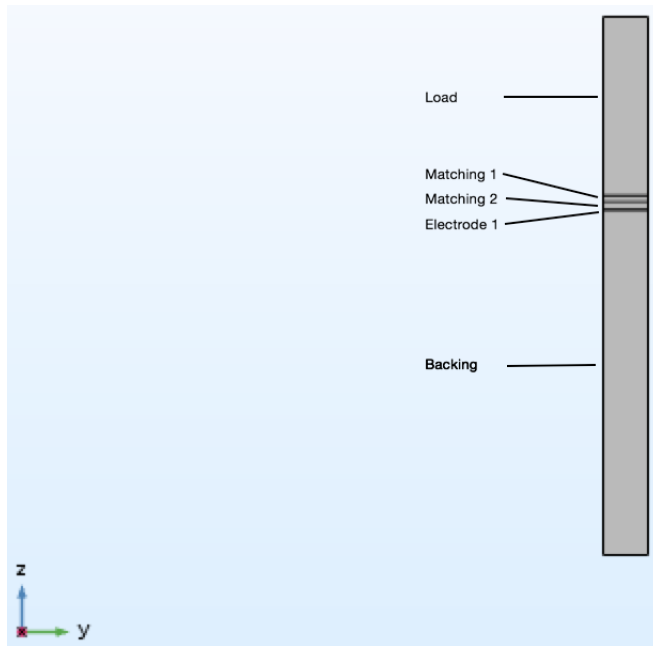


Figure 4.6: Transducer Geometry 3

In the simulations, we will measure the temperature distribution after 10 seconds of usage on the cross section line in the transducer from point $(0.01728, 2.5 \cdot 10^{-4}, 0)$ to point $(0.01728, 2.5 \cdot 10^{-4}, 0.0060263)$. This line is in the center of the transducer and where the temperature is highest. We are doing this to see the temperature in all the layers of the transducer and the line is shown in Figure 4.7.

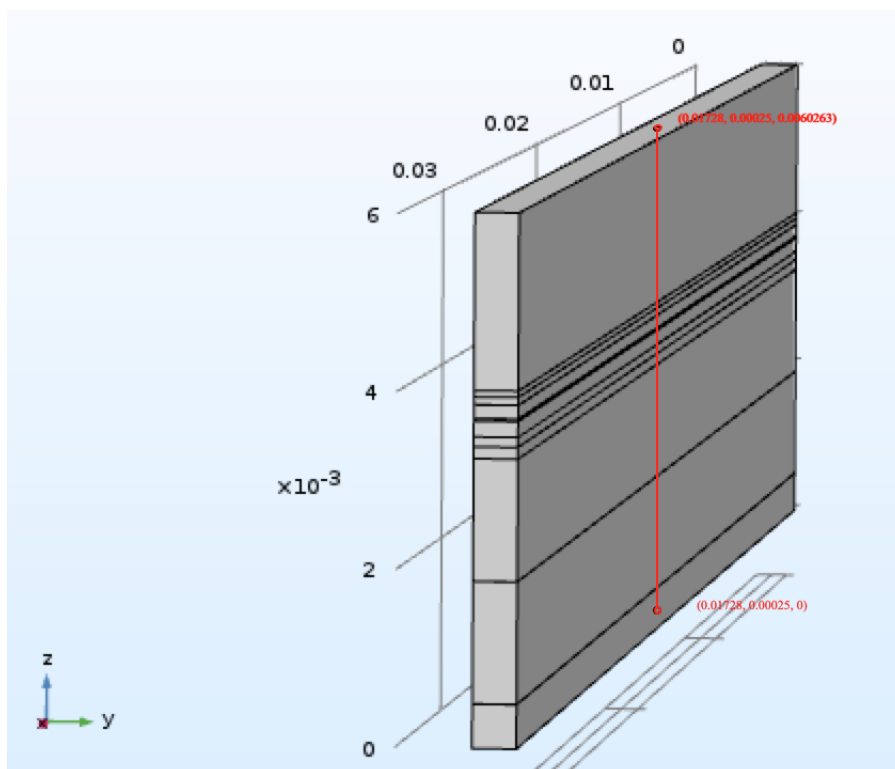


Figure 4.7: The red line represents the line from point $(0.01728, 2.5 \cdot 10^{-4}, 0)$ to $(0.01728, 2.5 \cdot 10^{-4}, 0.0060263)$

Also the temperature development in the plane $(x, 0.00025, z)$, which is the center of the transducer, will be simulated for the three geometries.

4.5.3 Cooling methods

As described in section 2.3.10 there are three ways to control the temperature of the transducer, active cooling, passive cooling or a combination. Because of the apparent cost and reliability issues it is preferable to use passive heat transfer methods to cool the transducer [Park et al., 2008]. Then there is no need for power, and service and reparations are minimized. Also because of the acoustic vibrations, there are very severe constraints on any potential transducer cooling means inside the transducer.

To cool the transducer (Geometry 1), we are starting with simulating the transducer with fans making the convection to the surroundings more effective. To do this in Comsol we are changing the boundary condition from natural to forced external convection with air, and a velocity of 2 m/s.

After that we are using a heat sink method that consists of copper slabs. We are putting two copper slabs on each side of the transducer to enhance heat transfer. Copper has good heat sink properties as described in Section 2.3.10. Figure 4.8 shows the transducer with copper slabs and the dimensions of the slabs are given in Table 4.2. The domain for the simulation is now the transducer and copper slabs. The boundary condition is air with a temperature of 298 K and no motion.

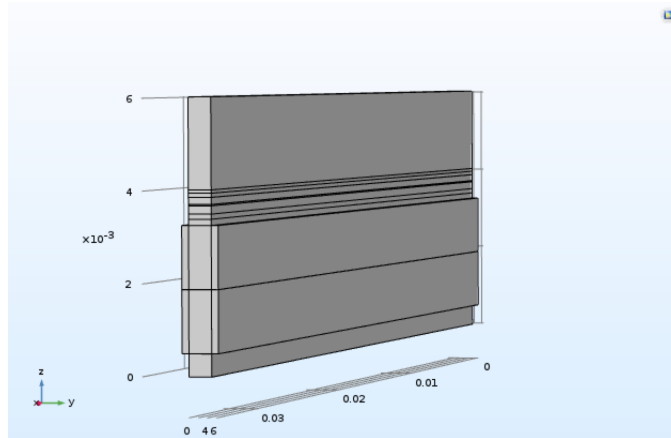


Figure 4.8: The geometry of the transducer with copper slabs

Table 4.2: Geometrical dimensions of the copper slabs

Number of slabs	Length (x-dim)	Depth (y-dim)	Height (z-dim)	Volume
4	34.56 mm	0.15 mm	1.3787 mm	7.15 mm ³
Total of all the slabs				28.6 mm ³

CHAPTER 4. THERMAL DESIGN: DEVELOPMENT AND ANALYSIS

5. Results

5.1 Heat generation

In this project we are dealing with a 9 MHz SURF probe. The acoustic energy absorption will work as heat sources in the transducer. These are calculated in x-trans and presented in Figure 5.1 and Table 5.1 in W/m^3 .

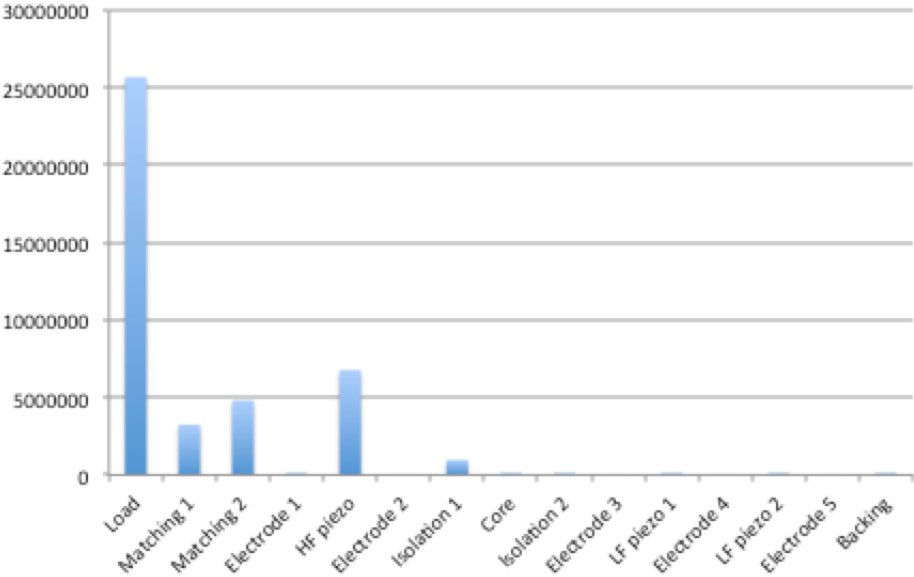


Figure 5.1: The heat sources in the different layers. The unit of the y-axis is W/m^3

Table 5.1: The heat sources in the different layers.

Layer	Heat source (W/m ³)
Load	25 675 551
Matching 1	3 243 582
Matching 2	4 814 798
Electrode 1	3372
HF piezo	6 767 017
Electrode 2	0
Isolation 1	960 937
Core	121 381
Isolation 2	138 240
Electrode 3	0
LF piezo 1	13 487
Electrode 4	0
LF piezo 2	3372
Electrode 5	0
Backing	3372

5.2 Heat development

When the transducer described in Figure 4.1 (Geometry 1) has operated for 10 seconds, the temperature distribution is as shown in Figure 5.2. The point with the highest temperature is $(0.01728, 2.5 \cdot 10^{-4}, 0.0060263)$ with a temperature of 381 K. In the following section this point is called point 1. This point is located in the load.

The warmest point in the transducer is $(0.01728, 2.5 \cdot 10^{-4}, 0.00402631)$ and this point is called point 2. This is on the face of the transducer and has a temperature of 336.8 K.

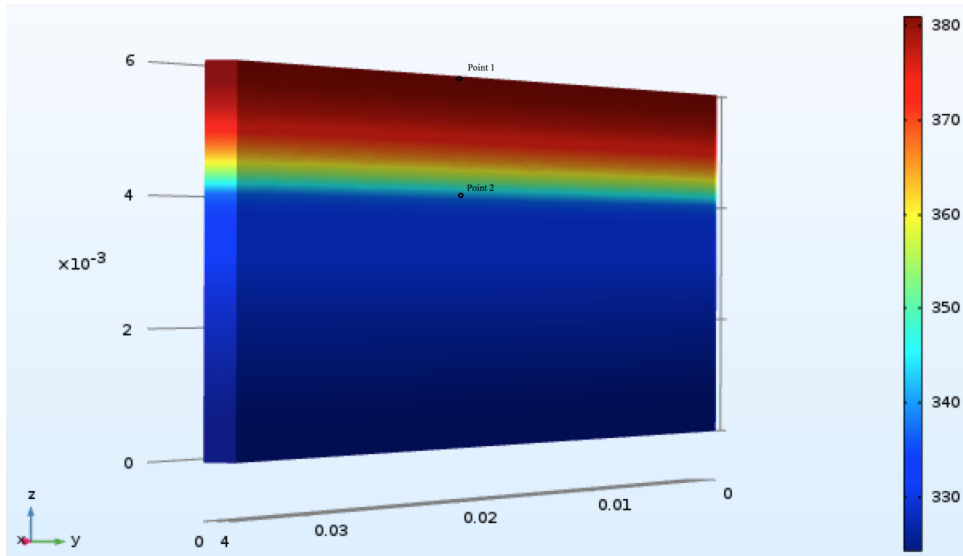


Figure 5.2: Temperature distribution in Kelvin in the transducer (Geometry 1) after operating for 10 seconds.

The temperature development of point 1 and point 2 from 0 to 10 seconds for Geometry 1 are shown in Figure 5.3.

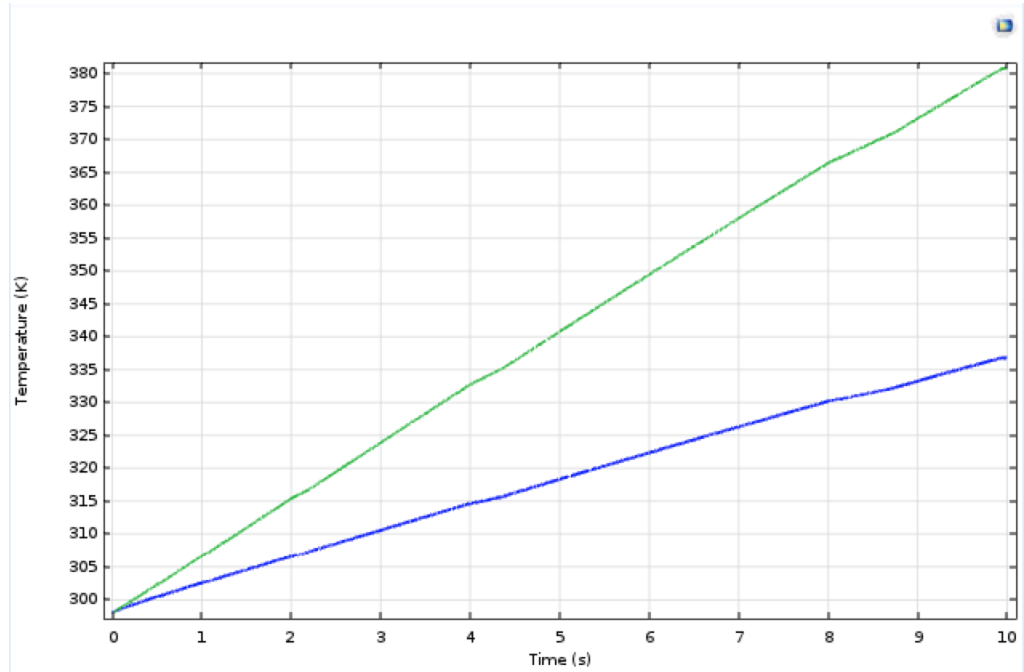


Figure 5.3: Temperature development in point 1 (blue line) and point 2 (green line).

5.3 The different geometries

For the three different geometries the temperature distribution in the cross section line, the heat generation and the temperature development in the inner xz-plane for the transducer are presented in the following section.

- The structure of Geometry 1 is shown in Figure 4.4 and the simulation results in Figure 5.4, 5.5 and 5.6.

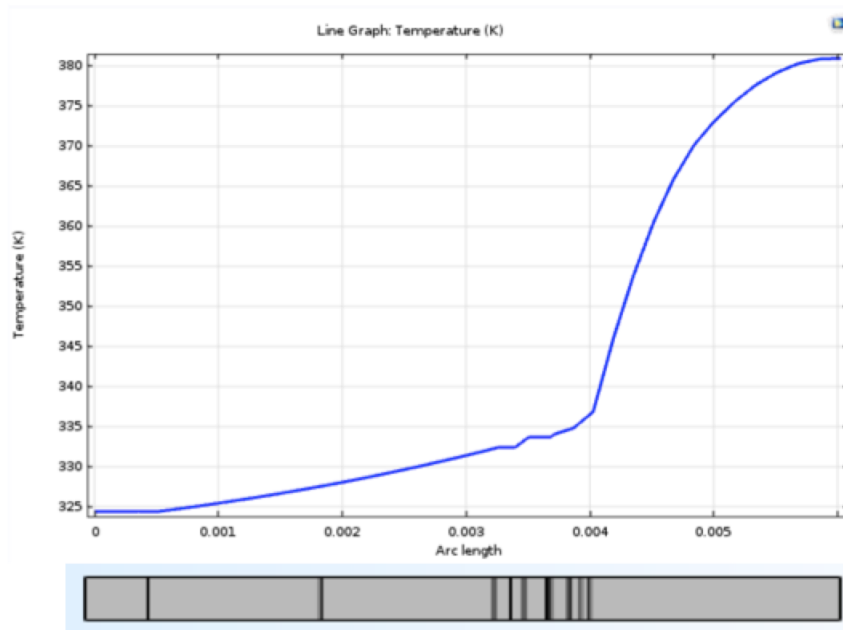


Figure 5.4: Temperature in the cross section line of Geometry 1 after operating for 10 seconds.

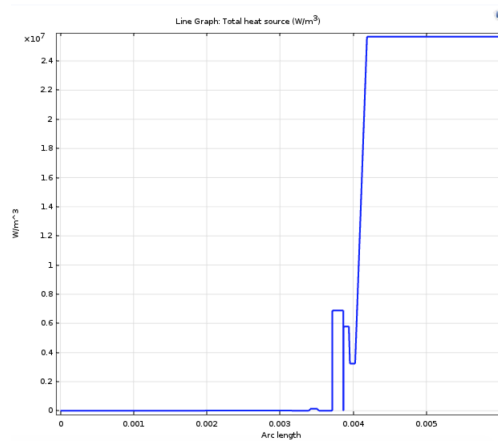


Figure 5.5: Heat generation in the cross section line of Geometry 1.

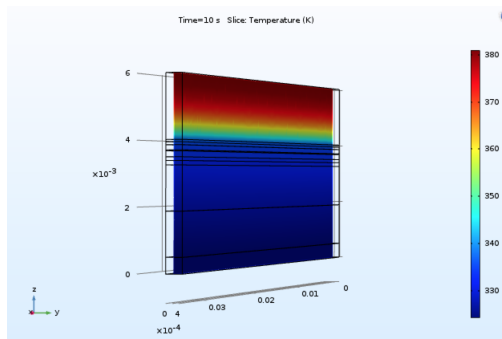


Figure 5.6: Temperature distribution after 10 *seconds* of usage in the xz-plane at $y = 25 \mu\text{m}$ of geometry 1

- The structure of Geometry 2 is shown in Figure 4.5 and the simulation results in Figure 5.7, 5.8 and 5.9.

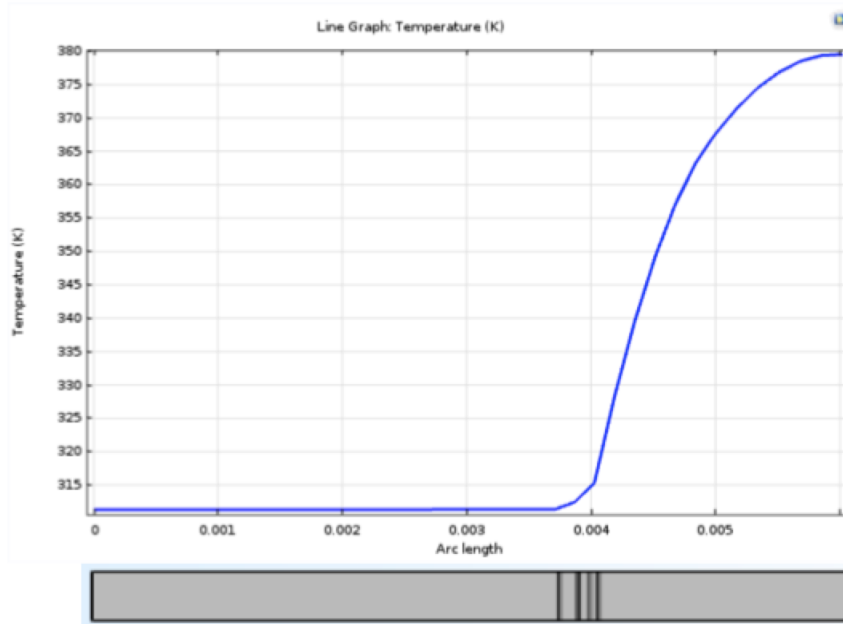


Figure 5.7: Temperature in the cross section line of Geometry 2 after operating for 10 seconds

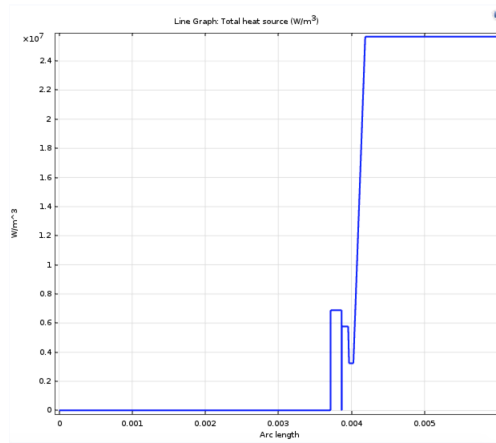


Figure 5.8: Heat generation in the cross section line of Geometry 2.

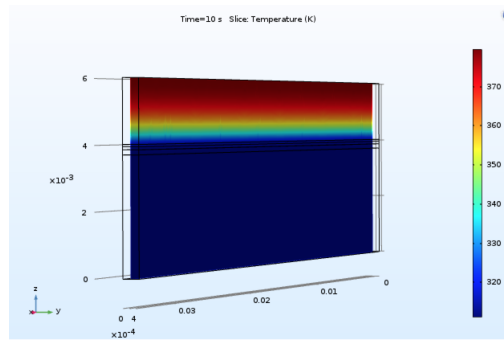


Figure 5.9: Temperature distribution after 10 seconds of usage in the xz-plane at 25 μm of geometry 2

CHAPTER 5. RESULTS

- The structure of Geometry 3 is shown in Figure 4.6 and the simulation results in Figure 5.10, 5.11 and 5.12.

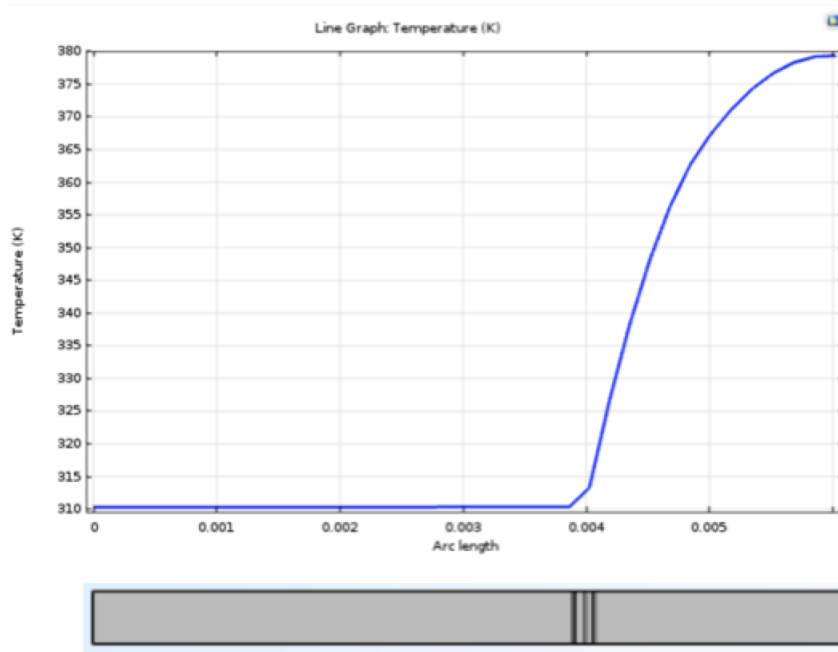


Figure 5.10: Temperature in the cross section line of Geometry 3 after operating for 10 seconds

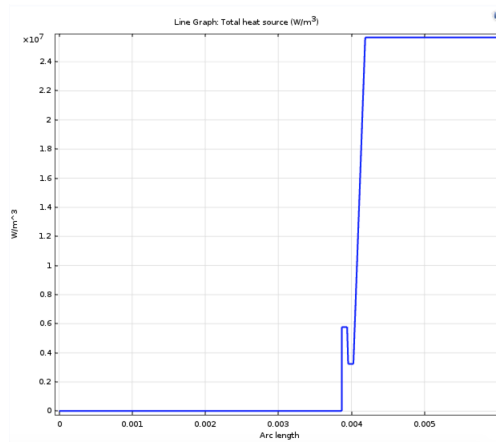


Figure 5.11: Heat generation in the cross section line of Geometry 3.

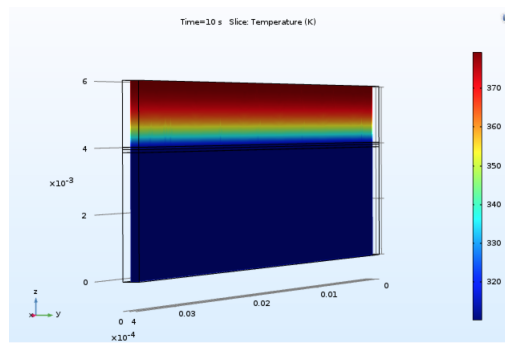


Figure 5.12: Temperature distribution after 10 *seconds* of usage in the xz-plane at 25 μm of geometry 3

5.4 Transducer with fans

The transducer with fans are described in Section 4.5.3 and the temperature distribution in point 1 and 2 are shown in Figure 5.13. The temperature development in the inner xz-plane are then presented along with the temperature in the cross section line.

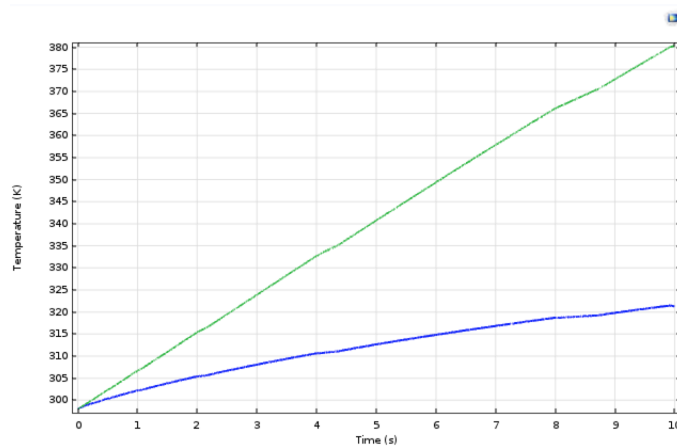


Figure 5.13: Temperature development in point 1 (blue line) and point 2 (green line) in the first 10 seconds of usage for the transducer (Geometry 1) with fans.

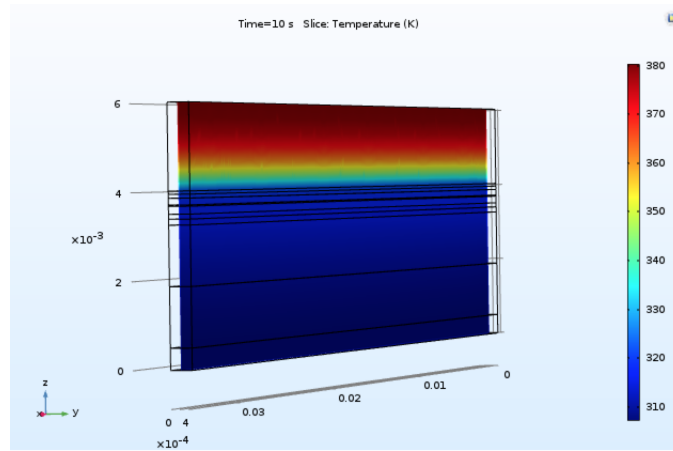


Figure 5.14: Temperature distribution after 10 seconds of usage in the inner xz-plane of the transducer (Geometry 1) with fans.

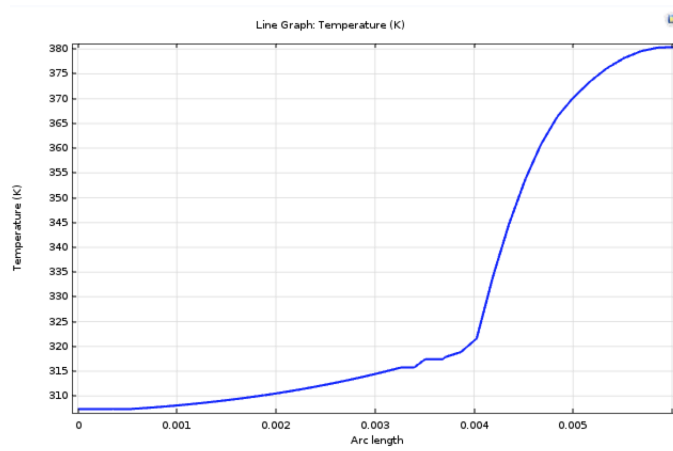


Figure 5.15: Temperature in the cross section line of the transducer (Geometry 1) with fans after operating for 10 seconds.

5.4.1 Transducer with copper slabs

Temperature distributions for the transducers with copper slabs, described in section 4.5.3, are presented in this section. The results are shown in Figure 5.16, 5.17 and 5.18.

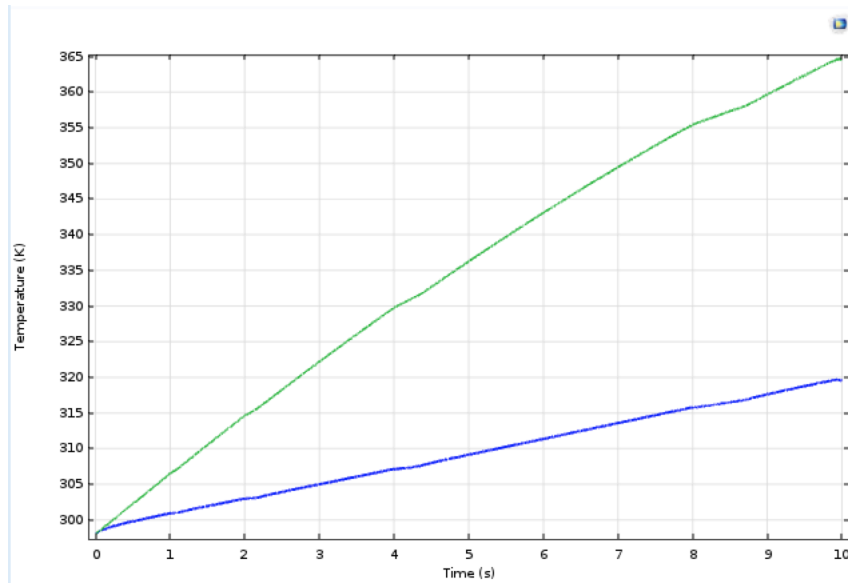


Figure 5.16: Temperature development in Point 1 (blue line) and Point 2 (green line) in the first 10 seconds of usage for the transducer (Geometry 1) with copper slabs.

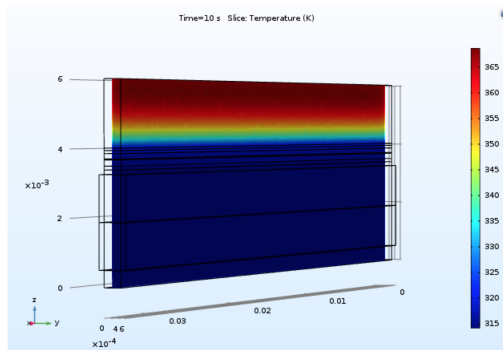


Figure 5.17: Temperature distribution after 10 seconds of usage in the xz -plane at $y = 25 \mu\text{m}$ of the transducer (Geometry 1) with copper slabs.

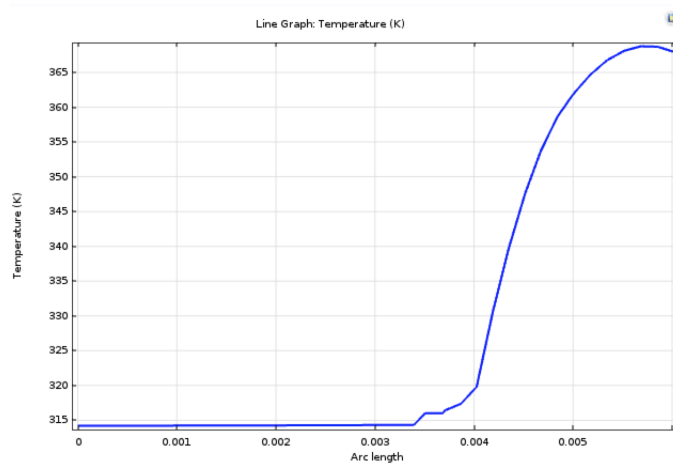


Figure 5.18: Temperature in the cross section line of the transducer (Geometry 1) with copper slabs after operating for 10 seconds.

CHAPTER 5. RESULTS

To summarize, the temperature in point 1 and 2 after 10 seconds of usage for all the cases are presented in Table 5.2.

Table 5.2: Temperature in point 1 and 2, in the different simulations

	Temperature point 1 [K]	Temperature point 2 [K]
Geometry 1	381	336.8
Geometry 2	379.4	315.3
Geometry 3	379.4	310.3
Transducer with fans	380.5	321.7
Transducer with slabs	366.8	314.2

CHAPTER 5. RESULTS

6. Discussion

6.1 Steady-state

Figure 5.3, which represents the temperature development in Point 1 and point 2 for geometry 1, shows that after 10 seconds the temperature is still increasing and it does not look like the plot has an asymptote either. After 10 seconds the temperature in Point 1 is as high as 381 K and the temperature in Point 2 is 336.8 K . From this simulation we can say that the temperature development in this period of time is transient or unsteady, as described in Section 2.3.3. The system has a change in operating condition due to internal energy generation, and this is larger than the convection rate with the surroundings as described in Equation 2.52.

6.2 Estimation of heat loss

To see if a potential cooling system of the transducer would be effective we are going to calculate how much heat which is lost to the environment. To do that, we are using the heat diffusion equation 2.52, rewritten as

$$Q + Q_{\text{loss}} = Q_{\text{generated}}, \quad (6.1)$$

where $Q_{\text{generated}}$ is evaluated in Comsol as 267 J. To find Q , I am going to do an approximation and using Equation 2.46. The mass of the transducer is 0.0047 kg. An average c_p value of the total structure is 600 J/kgK and the temperature increase, ΔT , in 10 seconds is 83 K. Then

$$Q = 0.0047 \cdot 600 \cdot 83 = 235J, \quad (6.2)$$

and, I can calculate Q_{loss} as

$$Q_{\text{loss}} = 267J - 235J = 32J \quad (6.3)$$

The loss in percent is

$$\frac{32J}{235J} \cdot 100 = 11.8\%. \quad (6.4)$$

To cool the transducer we need to increase this heat loss. There are several ways to do this as described in Section 4.5.3.

6.3 The limiting factors of heat transfer

The highest temperatures in the structure are in the load and close to the load as shown in Figure 5.2, where also the heat sources are largest as Figure 5.1 shows. The largest heat source is in the load, followed by the HF layer and the matching layers. To cool the transducer it is important to lead heat from these layers. The critical parameter in limiting internal temperature is then the heat source in the load. It is difficult to have any cooling system in the load. After all, it is the body of the patient.

6.4 Influence of the materials

Table 5.2 shows the temperature of all the simulations in point 1 and 2. Geometry 1 has the highest maximum temperature in point 1, followed by geometry 2 and geometry 3. For all three geometries the highest temperature of the structure is located on the face. This temperature, however, is not very different in the geometries. Geometry 1 has a temperature which is 1.6 K higher than Geometry 2 and 3.

In point 2, the end of the transducer, there is a larger difference. Geometry 1 has an approximate linear temperature rise from the backing layer to the matching 1 layer. This results in a temperature of $336.8K$ in point 2 compared to $315 K$ in Geometry 2 and $310.3 K$ in Geometry 3.

It is clear from Section 2.3.1 that the ideal material to cool the transducer has high conductivity, which enhance the conductive heat transfer. The material in the backing layer is copper, which has a high thermal conductivity. Followed by a small heat source the backing layer has the lowest temperature in the transducer in the three geometries, and the temperature is constant through the whole layer. Geometry 2 and geometry 3 have a larger backing layer than geometry 1, and a larger area of the transducer has a lower temperature.

In Geometry 2 and 3 the temperature is slightly higher in the HF Piezo and matching layers than in the backing layer. Also, the temperature in the matching layers are higher in Geometry 2 than in Geometry 1, but this is not considerable. The real temperature rise happens in the load.

The material properties of the transducer does not influence the convective heat transfer directly. As described in Section 2.3.5, the properties of the transducer material are not part of the convective heat equations. Convection depends only on the temperature at the surface, the area of the surface, the temperature of the surroundings and the convection heat transfer coefficient of the surrounding fluid. However, the material properties influence the conductive heat transfer in the transducer and to the surface.

6.5 Influence of the fans

When comparing Figure 5.4 with Figure 5.15 we can see that the temperature is lower in all the layers in the transducer stack when fans are used. As Figure 5.13 also shows, the temperature increase in Point 2 is more slow using fans compared to Figure 5.3. After 10 seconds, the temperature in Point 2 is 321.7 K with fans, compared to 336.8 K without.

However, the fans can only be used on the transducer stack, and not on the load. The temperature in point 1 is only 0.5 K lower than geometry 1, so the fans are not making the load cooler. Also, because this is an active cooling solution it needs power to run and that is a disadvantage of this method.

6.6 Influence of the copper slabs

The use of copper slabs are effective for cooling the transducer, more effective than the use of fans when comparing Figure 5.16 with Figure 5.13. After 10 seconds the temperature in point 2 with copper slabs is 314.2 K, which is also lower than the temperature of geometry 2 as Table 5.2 shows. The temperature in point 1 is also considerably lower for the transducer with copper slabs than all the other cases.

The use of copper slabs is a passive cooling system and the slabs cool the transducer by dissipating heat. This method is preferable because it does not need power to run. The copper slabs near the load is most important for cooling the transducer. In this area the temperature has its maximum and therefore it is important to enhance heat transfer there.

6.7 Radiation

In the simulations, radiation is neglected based on the assumptions in Section 4.3. We will in this section check the validation of these assumptions by comparing the convection and radiation heat rate.

From Comsol the convection heat rate at 10 seconds is

$$q_{\text{conv}} = 415 \text{ W/m}^2. \quad (6.5)$$

Large surroundings may be treated as hypothetical black surfaces. Because the absorptivity of a black surface is unity, there is no reflection and the radiosity consists only of the emitted energy. If the transducer is surface 1 and the surroundings are surface 2, Eqn. 2.92 then reduces to

$$q_{12} = F_{12}\epsilon_1\sigma(T_1^4 - T_2^4), \quad (6.6)$$

where σ is the Stefan-Boltzmann constant.

The view factor of a small object in an enclosure, $F_{12} = 1$ [Dewitt et al., 2007]. The transducer casing is typical plastic, but the emissivity also depends on the surface treatment. We will try a range of values from 0.2 to 1.0 for the transducer. We are also simplifying the equation, only using the temperature of the transducer.

With an emissivity of 0.2, 0.6 and 1.0, respectively, the radiation is

$$q_{\text{rad}} = 1 \cdot 0.2 \cdot 5.67 \cdot 10^{-8} \cdot (381)^4 = 239\text{W/m}^2, \quad (6.7)$$

$$q_{\text{rad}} = 1 \cdot 0.6 \cdot 5.67 \cdot 10^{-8} \cdot (381)^4 = 717\text{W/m}^2, \quad (6.8)$$

and

$$q_{\text{rad}} = 1 \cdot 1.0 \cdot 5.67 \cdot 10^{-8} \cdot (381)^4 = 1195\text{W/m}^2. \quad (6.9)$$

The radiation emission is strongly depending on the emissivity of the transducer. With a high value, the radiation heat transfer is larger than the convective heat transfer and the influence of radiation has to be considered.

7. Conclusion

In this thesis the main purpose has been studying heat sources and heat transfer in vibrating high power, multifrequency transducers to be used for both ultrasound imaging and for mediation of drug delivery.

An ultrasound transducer generates plane, longitudinal pressure waves. In this acoustic wave motion, energy is converted to other energy forms, like heat energy. The finite element program Comsol was used for these heat generation simulations.

The area with the highest temperature in the transducer would be on top of the matching layers with a temperature of 336.8 K, based on the results. By studying different geometries, some of the transducer layers effect on the heat generation were tested. The geometry with the largest backing layer had the lowest maximum temperature in the transducer, with a value of 310.3 K.

Some methods for limiting the internal temperature of the transducer were then proposed. First, an active cooling method using fans was tested. Then, the use of copper slabs, which is a passive cooling method to enhance heat transfer, was simulated. Based on Geometry 1, the transducer with slabs was most effective when it came to cooling the transducer. The maximum temperature in the transducer was lowered to 314.2 K.

However, based on the simulations, the real problem is the heat generation in the load. In the first simulation the highest temperature in the load was 381 K and with copper slabs, the maximum temperature was measured as 366.8 K. This area can be hard to make cooler. The heat properties of the load could be chosen different to make the temperature rise smaller, but this effect would probably not be considerable. For further studies it is important to find ways cooling the load.

CHAPTER 7. CONCLUSION

Bibliography

- [HIF, 2015] (2015). High intensity focused ultrasound (hifu). <http://www.cancerresearchuk.org/about-cancer/cancers-in-general/treatment/other/high-intensity-focused-ultrasound-hifu>. Accessed: 2015-08-20.
- [Angelsen, 2000] Angelsen, B. A. (2000). *Ultrasound imaging: Waves Signals and Signal Processing*.
- [Ashby and Lu, 2003] Ashby, M. F. and Lu, T. (2003). Metal foams: a survey. *Science in China Series B: Chemistry*, 46(6):521–532.
- [Cole et al., 2011] Cole, A. J., Yang, V. C., and David, A. E. (2011). Cancer theranostics: the rise of targeted magnetic nanoparticles. *Trends in biotechnology*, 29(7):323–332.
- [Comsol, 2016] Comsol (2016). What is multiphysics?
- [Dewan et al., 2004] Dewan, A., Mahanta, P., Raju, K. S., and Kumar, P. S. (2004). Review of passive heat transfer augmentation techniques. *Proceedings of the Institution of Mechanical Engineers, Part A: Journal of Power and Energy*, 218(7):509–527.
- [Dewitt et al., 2007] Dewitt, D., Incropera, F., Lavine, A., and Begman, T. (2007). *Fundamentals of Heat and Mass Transfer, 7th edition*.
- [Duck, 2013] Duck, F. A. (2013). *Physical properties of tissues: a comprehensive reference book*. Academic press.
- [Eggen et al., 2014] Eggen, S., Fagerland, S.-M., Mørch, Ý., Hansen, R., Søvnik, K., Berg, S., Furu, H., Bøhn, A. D., Lilledahl, M. B., Angelsen, A., et al. (2014). Ultrasound-enhanced drug delivery in prostate cancer xenografts by nanoparticles stabilizing microbubbles. *Journal of Controlled Release*, 187:39–49.
- [Giering et al., 1996] Giering, K., Lamprecht, I., and Minet, O. (1996). Specific heat capacities of human and animal tissues. In *BiOS Europe '95*, pages 188–197. International Society for Optics and Photonics.

BIBLIOGRAPHY

- [Hart, 2006] Hart, J. (2006). Ultrasound transducer assembly having improved thermal management. US Patent App. 11/912,617.
- [He, 2004] He, Y. (2004). Heat capacity, thermal conductivity, and thermal expansion of barium titanate-based ceramics. *Thermochimica Acta*, 419(1):135–141.
- [Hooker, 1998] Hooker, M. W. (1998). Properties of pzt-based piezoelectric ceramics between-150 and 250 degrees celsius.
- [Hubert, 1972] Hubert, H. (1972). Peltier-effect heat pump. US Patent 3,635,037.
- [Huebner et al., 2001] Huebner, K. H., Dewhirst, D. L., Smith, D. E., and Byrom, T. G. (2001). *The Finite Element Method for Engineers, (Golden, United States)*. John Wiley sons, inc.
- [Jiji, 2009] Jiji, L. M. (2009). Transient conduction. In *Heat Conduction*, pages 119–162. Springer.
- [Kaneko and Willmann, 2012] Kaneko, O. F. and Willmann, J. K. (2012). Ultrasound for molecular imaging and therapy in cancer. *Quantitative imaging in medicine and surgery*, 2(2):87–97.
- [Kennedy, 2005] Kennedy, J. E. (2005). High-intensity focused ultrasound in the treatment of solid tumours. *Nature Reviews Cancer*, 5(4):321–327.
- [Knight et al., 1991] Knight, R., Goodling, J., and Hall, D. (1991). Optimal thermal design of forced convection heat sinks-analytical. *ASME J. Electron. Packag*, 113(3):313–321.
- [Léal et al., 2013] Léal, L., Miscovic, M., Lavieille, P., Amokrane, M., Pigache, F., Topin, F., Nogarède, B., and Tadrist, L. (2013). An overview of heat transfer enhancement methods and new perspectives: Focus on active methods using electroactive materials. *International Journal of Heat and Mass Transfer*, 61:505–524.
- [Lienhard, 2013] Lienhard, J. H. (2013). *A Heat Transfer Textbook. (Boston, United States)*. Courier Corporation.
- [Liu and Sakr, 2013] Liu, S. and Sakr, M. (2013). A comprehensive review on passive heat transfer enhancements in pipe exchangers. *Renewable and Sustainable Energy Reviews*, 19:64–81.
- [Mangum and Hill, 1977] Mangum, B. W. and Hill, J. E. (1977). Thermal analysis–human comfort–indoor environments. nbs special publication 491.
- [Miller et al., 2012] Miller, D. L., Smith, N. B., Bailey, M. R., Czarnota, G. J., Hynynen, K., and Makin, I. (2012). Overview of therapeutic ultrasound applications and safety considerations. *Journal of Ultrasound in Medicine*, 31(4):623–634.

BIBLIOGRAPHY

- [Park et al., 2008] Park, W. J., Marian, V., Petersen, D., Sheljaskow, T., Bolorosh, M. S., Walters, W. B., and Ayter, S. (2008). System and method for actively cooling transducer assembly electronics. US Patent 7,314,447.
- [Partlov, 2015] Partlov (2015). Unsteady conduction heat transfer.
- [Poppendiek et al., 1967] Poppendiek, H., Randall, R., Breeden, J., Chambers, J., and Murphy, J. (1967). Thermal conductivity measurements and predictions for biological fluids and tissues. *Cryobiology*, 3(4):318–327.
- [Sadrizadeh and Holmberg, 2015] Sadrizadeh, S. and Holmberg, S. (2015). How safe is it to neglect thermal radiation in indoor environment modeling with high ventilation rates? In *AIVC*, page 436.
- [Szabo, 2004] Szabo, T. L. (2004). *Diagnostic ultrasound imaging: inside out*. Academic Press.
- [Ugelstad et al., 1985] Ugelstad, J., Mfutakamba, H., Mørk, P., Ellingsen, T., Berge, A., Schmid, R., Holm, L., Jørgedal, A., Hansen, F., and Nustad, K. (1985). Preparation and application of monodisperse polymer particles. In *Journal of Polymer Science: Polymer Symposia*, volume 72, pages 225–240. Wiley Online Library.
- [Zhang et al., 2008] Zhang, H., Zhang, X., and Zheng, L. (2008). An analysis of the characteristics of the thermal boundary layer in power law fluid. *Journal of Thermal Science*, 17(3):233–237.
- [Zhang et al., 2017] Zhang, Y., Xie, M., Roscow, J., Bao, Y., Zhou, K., Zhang, D., and Bowen, C. R. (2017). Enhanced pyroelectric and piezoelectric properties of pzt with aligned porosity for energy harvesting applications. *Journal of Materials Chemistry A*, 5(14):6569–6580.
- [Zhou et al., 2014] Zhou, Q.-L., Chen, Z.-Y., Wang, Y.-X., Yang, F., Lin, Y., and Liao, Y.-Y. (2014). Ultrasound-mediated local drug and gene delivery using nanocarriers. *BioMed research international*, 2014.